

2m4

CR 114711
AVAILABLE TO THE PUBLIC

CONCEPTS FOR A THEORETICAL AND EXPERIMENTAL
STUDY OF LIFTING ROTOR RANDOM
LOADS AND VIBRATIONS

(Further Experiments with Progressing/Regressing
Rotor Flapping Modes)

Phase VII-C Report under Contract NAS2-4151

by

Kurt H. Hohenemser

and

S. T. Crews

NASA-CR-114711)	CONCEPTS FOR A	N74-14759
THEORETICAL AND EXPERIMENTAL STUDY OF		
LIFTING ROTOR RANDOM LOADS AND VIBRATIONS		
(FURTHER EXPERIMENTS WITH (Washington		Unclas
Univ.) 76 p HC \$6.00	CSCL 01C	G3/02 26991

Department of Mechanical and
Aerospace Engineering



Washington University
School of Engineering and Applied Science
St. Louis, Missouri

June, 1973

CONCEPTS FOR A THEORETICAL AND EXPERIMENTAL
STUDY OF LIFTING ROTOR RANDOM
LOADS AND VIBRATIONS

(Further Experiments with Progressing/Regressing
Rotor Flapping Modes)

Phase VII-C Report under Contract NAS2-4151

Prepared for the Ames Directorate, AMRDL, at
Ames Research Center, Moffett Field, California

by Kurt H. Hohenemser

Kurt H. Hohenemser

and S. T. Crews

S. T. Crews

Washington University
School of Engineering and Applied Science
St. Louis, Missouri

June, 1973

Reports and Publications UnderContract NAS2-4151

The following reports under subject research contract have been submitted:

1. Phase I Report of September 1967, Analytical Concepts for a Random Loads and Vibration Analysis of Lifting Rotors.
2. Phase II Report of August 1968, Perturbation Solution Method for Random Blade Flapping.
3. Phase III Report of June 1969, Random Blade Flapping Response to Atmospheric Turbulence at High Advance Ratio.
4. Phase IV Report of June 1970, Threshold Crossing Statistics for Rotor Blade Random Flapping.
5. Phase V-A Report of June 1971, Effects of Torsional Blade Flexibility on Single Blade Random Gust Response Statistics.
6. Phase V-B Report of June 1971, Analysis of Gust Alleviation Methods on Rotor Dynamic Stability.
7. Phase V-C Report of June 1971, Development of Experimental Methods in Support of the Analysis.
8. Phase VI-A Report of June 1972, Part I, Random Gust Response Statistics for Coupled Torsion-Flapping Rotor Blade Vibrations.
Part II, Flap Bending Corrections to the Rigid Blade Analysis of Lifting Rotors.
Part III, Effects of Rotor Support Flexibility.
9. Phase VI-B Report of June 1972, Experiments with Progressing/Regressing Forced Rotor Flapping Modes.
10. Phase VII-A Report of June 1973, The Effects of Some Rotor Feedback Systems on Rotor-Body Dynamics.
11. Phase VII-B Report of June 1973, Identification of Lifting Rotor System Parameters from Transient Response Data.
12. Phase VII-C Report of June 1973, Further Experiments with Progressing/Regressing Rotor Flapping Modes.

The following papers and articles sponsored under subject research contract have been published to date:

1. Gaonkar, G. H. and Hohenemser, K. H., "Flapping Response of Lifting Rotor Blades to Atmospheric Turbulence", Journal of Aircraft, Vol. 6, Nov.-Dec. 1969, pp. 496-503. First presented as AIAA Paper 69-206 at the AIAA/AHS VTOL Meeting, Atlanta, Georgia, February 1969.
2. Gaonkar, G. H. and Hohenemser, K. H., "Stochastic Properties of Turbulence Excited Rotor Blade Vibrations", AIAA Journal, Vol. 9, No. 3, March 1971, pp. 419-424. First presented as AIAA Paper 70-548 at the AIAA Atmospheric Flight Mechanics Conference, Tullahoma, Tennessee, May 1970.
3. Gaonkar, G. H. and Hohenemser, K. H., "Comparison of Two Stochastic Models for Threshold Crossing Studies of Rotor Blade Flapping Vibrations", presented as AIAA Paper 71-389 at the AIAA/ASME 12th Structures Conference, Anaheim California, April 1971.
4. Yin, S. K. and Hohenemser, K. H., "The Method of Multiblade Coordinates in the Linear Analysis of Lifting Rotor Dynamic Stability and Gust Response", presented as AHS Preprint No. 512 at the 27th Annual National Forum of the AHS, Washington, D.C., May 1971.
5. Hohenemser, K. H. and Yin, S. K., "Some Applications of the Method of Multiblade Coordinates", Journal of the American Helicopter Society, Vol. 17, No. 3, July 1972.
6. Gaonkar, G. H. and Hohenemser, K. H., "An Advanced Stochastic Model for Threshold Crossing Studies of Rotor Blade Vibrations", AIAA Journal, Vol. 10 No. 8, pp. 1100-1101, August 1972.
7. Prelewicz, D. A., "Response of Linear Periodically Time Varying Systems to Random Excitation", AIAA Journal, Vol. 10 No. 8, pp. 1124-1125, August 1972.
8. Hohenemser, K. H. and Crews, S. T., "Unsteady Wake Effects on Progressing/Regressing Forced Rotor Flapping Modes", AIAA 2nd Atmospheric Flight Mechanics Conference, Palo Alto, California. AIAA Paper No. 72-957, September 1972.
9. Gaonkar, G. H., Hohenemser, K. H., and Yin, S. K., "Random Gust Response Statistics for Coupled Torsion-Flapping Rotor Blade Vibrations", Journal of Aircraft, Vol. 9 No. 10, pp. 726-729, October 1972.

10. Hohenemser, K. H. and Crews, S. T., "Model Tests on Unsteady Rotor Wake Effects", Journal of Aircraft, Vol. 10 No. 1, pp. 58-60, January 1973.
11. Hohenemser, K. H. and Yin, S. K., "On the Question of Adequate Hingeless Rotor Modeling in Flight Dynamics", 29th Annual National Forum of the American Helicopter Society, Washington, D.C., Preprint No. 732, May 1973.

CONCEPTS FOR A THEORETICAL AND EXPERIMENTAL
STUDY OF LIFTING ROTOR RANDOM
LOADS AND VIBRATIONS

Phase VII-C

(Further Experiments with Progressing/Regressing
Rotor Flapping Modes)

by

Kurt H. Hohenemser

and

S. T. Crews

Washington University
St. Louis, Missouri

Abstract

The experiments with progressing/regressing forced rotor flapping modes reported earlier have been extended in several directions and the data processing method has been considerably refined. The 16 inch hingeless 2-bladed rotor model was equipped with a new set of high precision blades produced at Princeton which removed previously encountered tracking difficulties at high advance ratio, so that tests up to .8 rotor advance ratio could be conducted. In addition to data with 1.20 blade natural flapping frequency data at 1.10 flapping frequency were obtained. Outside the wind tunnel, tests with a ground plate located at different distances below the rotor were conducted while recording the dynamic downflow at a station .2R below the rotor plane with a hot wire anemometer. Data processing was automatized in such a way that the first 7 Fourier components of the periodic response

modulating function could be obtained including their standard deviations from several different tests. For zero advance ratio the test results are compared with analytical results including a dynamic wake representation. For non-zero advance ratio the dynamic wake was omitted in the analysis. In addition to the test data obtained to date, this report includes a description of work which has been accomplished in preparation of future dynamic rotor model testing.

CONCEPTS FOR A THEORETICAL AND EXPERIMENTAL
STUDY OF LIFTING ROTOR RANDOM
LOADS AND VIBRATIONS

Phase VII-C

(Further Experiments with Progressing/Regressing
Rotor Flapping Modes)

<u>Table of Contents</u>	<u>Page</u>
Nomenclature	vii
Introduction	1
Analytical Model for Zero Advance Ratio	3
Analytical Model for Non-Zero Advance Ratio	7
Rotor Model Modifications	10
Dynamic Rotor Downwash Measurements	12
Improvements in the Method of Data Processing	14
Discussion of Test Results	16
Accomplished Work Toward Future Experiments	19
A. Four Bladed Pitch Stirring Rotor	
B. Two-Dimensional Hovering Wake Survey	
Conclusions	22
References	23
Figure Captions	24
Figures	25
Appendix A:	66
Updated List of Purchased and Borrowed Equipment	

Nomenclature

A	Aerodynamic blade constant
A_{cn+} , A_{sn+} , A_{cn-} , A_{sn-}	Coefficients of Harmonics $\cos(n + \omega_f)$, $\sin(n + \omega_f)$, $\cos(n - \omega_f)$, $\sin(n - \omega_f)$
B	Tip loss factor
$C(t)$	Aerodynamic blade damping
$F_R(t) + iF_I(t)$	Complex valued periodic response modulating function
$F_{Rcn} + iF_{Icn}$, $F_{Rsn} + iF_{Isn}$ $ F_{cn} $, $ F_{sn} $	Complex valued Fourier coefficients Absolute values of complex Fourier coefficients
L	Inflow gain
R	Rotor radius
t	Non-dimensional time, unit $1/\Omega$
β	Flapping angle, positive up (line from rotor center to blade station at $.7R$)
γ	Blade Lock number for first mode moment equation (γ_m in Reference 6)
λ	Inflow angle, constant over radius (only considered for $\mu = 0$)
θ	Blade pitch angle, positive nose up
Ω	Rotor angular speed
ω_1 or P	Blade natural frequency, rotating, unit Ω
ω	Frequency of forced excitation, rotating reference system
ω_f	Frequency of forced excitation, fixed reference system
τ	Inflow time constant

ϕ_{cn} , ϕ_{sn} Arguments of complex valued
Fourier coefficients ψ

Blade azimuth angle

Superscripts

.

Time derivative

*

Equivalent quantity including
inflow

Subscripts

I , II

Multiblade variables

k

Variables for kth blade

o

Time average

n Ω

Time Fourier Components

Introduction

Previous tests with the 16 inch two bladed rotor model are described in References 1, 2, 3. The tests were all conducted with a blade natural flapping frequency of 1.20. The maximum rotor advance ratio tested was .4. When harmonically exciting a periodic linear system, the response is a product of the harmonic exciting function and a "modulating" function with the period of the periodic system parameters. This modulating function takes the place of the complex amplitude ratio for harmonic excitation of a constant parameter system. In the previous work only the first harmonic of the modulating function was evaluated which corresponds to rotor tilting. The zero, second etc. harmonics of the modulating function are also of importance and have been evaluated in the new data processing routine and compared to the corresponding analytical values obtained without considering dynamic rotor inflow. The previous test data represented averages over several excitation periods and proved to be well repeatable. The present data are taken over one period of excitation 3 to 7 times, so that not only the mean but also the standard deviation could be obtained.

Previously, tracking difficulties encountered at higher advance ratio prevented the testing of rotor advance ratios above .4. With the new higher precision blades from Princeton this difficulty was overcome. The new blades were also tested at higher rotor speed corresponding to a natural flapping frequency of 1.10 in addition to the rotor speed with flapping frequency 1.20. First results of a dynamic wake survey during the forced rotor excitation

were obtained for the case of zero advance ratio, using hot wire anemometry. Some progress has been made in analytical modeling of the dynamic wake at zero advance ratio. Based on the concept of a participating air volume, equations including the dynamic wake effect can be derived and the size of the participating air volume can be determined by comparison with test results. An analytical model including dynamic wake effects, suitable for correlation with the progressing/regressing flapping tests, was simultaneously derived by R. A. Ormiston at AMRDL and by the authors at Washington University. Considerable preparations for extending the tests in several directions have been made and are briefly reported in the last section.

Analytical Model for Zero Advance Ratio

We begin by briefly discussing the analytical models with which the test results will be compared. For zero advance ratio the analysis includes dynamic wake effects. Two parameters of the analytical model are left to be determined from the tests. For non-zero advance ratio dynamic wake effects are not included in the analysis. For zero advance ratio the unsteady wake computation is based on the concept of a participating air mass included in the cylindrical volume of radius R and height h . For an impermeable axially accelerated circular disk the theoretical value of the height over radius ratio of the participating air volume is $h/R = .85$. This value was found to be approximately valid for rotors subject to collective pitch ramp inputs, see Reference 4. For the problem of harmonic cyclic pitch inputs the participating air volume will also be assumed to be a cylinder with radius R , but the height h will be left open to be determined from test results.

For a three or more bladed rotor operating at zero advance ratio, assuming straight blades flexibly hinged at the rotor center, the multiblade equations in a non-rotating reference system are according to Reference 5

$$\ddot{\beta}_I + A\dot{\beta}_I + (\omega_1^2 - 1)\beta_I + 2\dot{\beta}_{II} + A\beta_{II} = A(\theta_{II} + \lambda_I) \quad (1)$$

$$-2\dot{\beta}_I - A\beta_I + \ddot{\beta}_{II} + A\dot{\beta}_{II} + (\omega_1^2 - 1)\beta_{II} = A(-\theta_I + \lambda_{II}) \quad (2)$$

Terms with the factor $A = B^4 \gamma/8$ represent aerodynamic hub moments. The multiblade variables with the subscripts I and II are related

to the single blade variables used in a rotating frame of reference by

$$\beta_k = \beta_0 + \beta_I \cos \psi_k + \beta_{II} \sin \psi_k \quad (3)$$

$$\theta_k = \theta_0 - \theta_I \sin \psi_k + \theta_{II} \cos \psi_k \quad (4)$$

$$\lambda_k = \lambda_0 + \lambda_I \cos \psi_k + \lambda_{II} \sin \psi_k \quad (5)$$

Assuming that $\lambda_I \ll \lambda_0$, $\lambda_{II} \ll \lambda_0$ one finds from the unsteady moment of momentum equations about pitching and rolling axes through the rotor center:

$$\lambda_I + \tau \dot{\lambda}_I = -L [\ddot{\beta}_I + (\omega_1^2 - 1)\beta_I + 2\dot{\beta}_{II}] \quad (6)$$

$$\lambda_{II} + \tau \dot{\lambda}_{II} = -L [\ddot{\beta}_{II} + (\omega_1^2 - 1)\beta_{II} - 2\dot{\beta}_I] \quad (7)$$

The inflow gain factor L is proportional to $1/\lambda_0 \gamma$, the time constant τ is proportional to Lh/R . The terms in brackets in equations (6) and (7) are equal to the aerodynamic pitching and rolling moments about the rotor center, as can be seen from Eqs. (1) and (2).

Performing the Fourier transforms of Eqs. (6) and (7) and inserting the transformed λ_I and λ_{II} into the Fourier transformed Eqs. (1) and (2), one finds that the effect of the dynamic inflow is equivalent to replacing in the equations without inflow the parameter $1/A$ by

$$1/A^* = (1/A) + L/(1 + i \omega_f \tau) \quad (8)$$

or equivalent to replacing the Lock number γ by

$$\gamma^* = \gamma/[1 + B^4 \gamma L / 8(1 + i \omega_f \tau)] \quad (9)$$

so that Eqs. (1) and (2) become

$$\beta_I(-\omega_f^2 + A^* i \omega_f + \omega_1^2 - 1) + \beta_{II}(2 i \omega_f + A^*) = A^* \theta_{II} \quad (10)$$

$$\beta_I(-2i\omega_f - A^*) + \beta_{II}(-\omega_f^2 + A^* i\omega_f + \omega_1^2 - 1) = -A^* \theta_I \quad (11)$$

Progressing and regressing unit excitation is given respectively by

$$\theta_I = \exp i\omega_f t, \quad \theta_{II} = \bar{} \exp i\omega_f t \quad (12)$$

For a different inflow distribution over the radius the same equations would be obtained with different inflow gain L . Since gain and time constant are to be determined experimentally the actual inflow distribution is properly taken care of. For a two-bladed rotor it is better to start with the use of a rotating frame.

It can be shown that Eqs. (1) and (2) are equivalent in a rotating frame to the single blade equation

$$\ddot{\beta} + A\dot{\beta} + \omega_1^2 \beta = A(\theta + \lambda) \quad (13)$$

where at $t = 0$ the blade is located aft. We use the same inflow model defined by the left hand sides of Eqs. (6) and (7) but replace the right hand sides by the proper pitching and rolling moments for a two-bladed rotor:

$$\lambda_I + \tau \dot{\lambda}_I = -2L(\ddot{\beta} + \omega_1^2 \beta) \cos t \quad (14)$$

$$\lambda_{II} + \tau \dot{\lambda}_{II} = -2L(\ddot{\beta} + \omega_1^2 \beta) \sin t \quad (15)$$

Eqs. (14) and (15) can be transformed into a rotating frame of reference by introducing the auxiliary variable[†]

$$\eta = -\lambda_{II} \cos t + \lambda_I \sin t \quad (16)$$

[†]Dr. R. A. Ormiston suggested the use of Eqs. (13) to (15) and solved them by the harmonic balance method. Dr. S. K. Yin suggested the transformation (16) and derived Eqs. (17) to (19) with a formally different but numerically identical result.

By multiplying Eqs. (14) and (15) by $\cos t$ and $\sin t$ respectively and adding them one obtains with Eq. (5) for $\lambda = \lambda_k - \lambda_0$:

$$\tau \dot{\lambda} + \lambda + \tau \eta = -2L(\ddot{\beta} + \omega_1^2 \beta) \quad (17)$$

By using the factors $\sin t$ and $-\cos t$ and adding:

$$\tau \lambda - \tau \dot{\eta} - \eta = 0 \quad (18)$$

The Fourier transforms of Eqs. (13), (17), (18) give

$$\begin{aligned} \beta/\theta = & [(\omega_1^2 - \omega^2)\{(1/A) + 2L(1 + \tau^2 + \omega^2\tau^2)/[(1 + \tau^2 - \tau^2\omega^2)^2 + 4\omega^2\tau^2]\}] \\ & + i\omega\{1 + 2L\tau(\omega_1^2 - \omega^2)(\tau^2 - \tau^2\omega^2 - 1)/(1 + \tau^2 - \tau^2\omega^2)^2 + 4\omega^2\tau^2\}^{-1} \end{aligned} \quad (19)$$

Eq. (19) was used to correlate with test results, whereby the constants L and τ were selected in such a way as to obtain a reasonable correlation.

Analytical Model for Non-Zero advance Ratio

The analytical data for non-zero advance ratio, which are shown together with the test results, have been obtained with the single elastic mode analysis described in Reference (6). The parameters assumed for the model are:

Lock number for first mode moment equation $\gamma = 4.0$

Tip loss factor $B = .97$

Mode shape factor $\kappa = .087$

The flapping angle β is defined by the line from the rotor center to the blade station at $.7 R$, see Fig. 5 of Reference 1. The blade flap bending moment at the strain gauge per degree of flapping angle is as before

$$M_s/\beta = .062 \text{ in lbs/0}$$

Up to advance ratio of $.6$ the reversed flow effect was neglected, for $\mu = .8$ it was included.

With ω_f designating the frequency of progressing or regressing in a non-rotating frame of reference, the blade pitch excitation for progressing is in a rotating frame, assuming unit pitch amplitude

$$\theta = \exp it(1 - \omega_f) = (\cos t + i \sin t) \exp(-it\omega_f) \quad (20)$$

The equation of flapping motion is

$$\begin{aligned} (1/\gamma)\ddot{\beta} + (1/2) C(t) \dot{\beta} + (1/\gamma) \omega_1^2 \beta + (1/2) K(t) \beta \\ = (1/2) m_\theta(t)(\cos t + i \sin t) \exp(-it\omega) \end{aligned} \quad (21)$$

The functions $C(t)$, $K(t)$, $m_\theta(t)$ are periodic with period 2π and are defined in Reference 4. The flapping response is of the form

$$\beta = [F_R(t) + i F_I(t)] \exp(-i\omega_f t)$$

where the functions $F_R(t)$ and $F_I(t)$ are real functions with period 2π . The complex periodic function $F_R(t) + i F_I(t)$ takes for a periodic system the place of the complex response amplitude of a constant system. We denote it the response modulating function. Expanding this function in a Fourier series

$$F_R(t) + i F_I(t) = \sum_{n=0}^{\infty} [(F_{Rcn} + i F_{Icn}) \cos nt + (F_{Rsn} + i F_{Isn}) \sin nt] \quad (22)$$

the response problem is solved if the complex coefficients of this Fourier series are determined. One way of doing this is to take the real parts of input and response

$$\theta = \cos(1 - \omega_f)t \quad (23)$$

$$\begin{aligned} \beta = \sum_{n=0}^{\infty} & (F_{Rcn} \cos nt \cos \omega_f t + F_{Rsn} \sin nt \cos \omega_f t \\ & + F_{Icn} \cos nt \sin \omega_f t + F_{Isn} \sin nt \sin \omega_f t) \end{aligned} \quad (24)$$

The response can also be written in the form

$$\begin{aligned} \beta = \sum_{n=0}^{\infty} & [A_{cn+} \cos(n + \omega_f)t + A_{sn+} \sin(n + \omega_f)t \\ & + A_{cn-} \cos(n - \omega_f)t + A_{sn-} \sin(n - \omega_f)t] \end{aligned} \quad (25)$$

By equating coefficients of harmonics we have

$$\begin{aligned}
 F_{Rcn} &= A_{cn+} + A_{cn-} , F_{Rsn} = A_{sn+} + A_{sn-} \\
 F_{Icn} &= A_{sn+} - A_{sn-} , F_{Isn} = A_{cn-} - A_{cn+} \\
 n &= 0, 1, 2 \dots
 \end{aligned}
 \tag{26}$$

One has to determine from the flapping response to $\theta = \cos(1 - \omega_f)t$ the Fourier coefficients for the harmonics $n + \omega$ and $n - \omega$, and then use the preceding equations to obtain the Fourier coefficients of the response modulating function $F_R(t) + i F_I(t)$.

The equivalent to an absolute response amplitude of a constant system are the absolute values of the complex Fourier coefficients of the response modulating function $F_R(t) + i F_I(t)$. They are defined by

$$|F_{cn}| = (F_{Rcn}^2 + F_{Icn}^2)^{1/2}, \quad |F_{sn}| = (F_{Rsn}^2 + F_{Isn}^2)^{1/2}, \quad n = 0, 1, 2, \dots
 \tag{27}$$

$|F_{co}|$ is the coning amplitude, $|F_{cl}|$ and $|F_{sl}|$ are forward and left rotor tilting amplitudes, the higher order terms are rotor warping amplitudes. The test results will be mainly presented in terms of $|F_{cn}|$ and $|F_{sn}|$ for $n = 0$ to 3 and compared to the corresponding analytical values. The equivalent to the response phase angle of constant coefficient systems are the arguments of the complex valued Fourier coefficients

$$\begin{aligned}
 \phi_{cn} &= \text{ang}(F_{Rcn} + i F_{Icn}) \\
 \phi_{sn} &= \text{ang}(F_{Rsn} + i F_{Isn})
 \end{aligned}
 \tag{28}$$

Plotted and compared to analytical values will only be the phase angles ϕ_{cl} and ϕ_{sl} which represent the phase relation between rotor tilting response and cyclic pitch input.

Rotor Model Modifications

All data presented in this report were obtained with the rotor model described in Reference 1 modified in the following way:

1. The oilyte hub bearings were replaced by microprecision bearings.
2. A phase measuring tool was added to obtain a better adjustment of the blade pitch excitation phase angle.
3. The collective pitch adjustment and tracking procedure were improved by adjustment tools.
4. Blade torsion strain gauges were installed. The torsion response was recorded but not as yet evaluated.
5. Precision rotor blades built by W. Putnam Co. of Princeton, New Jersey were installed together with new blade retentions and new blade flexures.

As compared to the previous blades the new blades have the following natural frequencies without rotation:

	New Blades	Previous Blades
First flapwise frequency	12.5 cps	11.7 cps
Second flapwise frequency	150	153
Torsion frequency	205	190
Edgewise frequency	160	(120)

The difference in first flapwise frequency is caused by a slight difference in the thickness of the flexure. The approximate equality of the second flapwise and of the torsion natural frequencies indicate good dynamic similarity between the two sets of

blades. The edgewise natural frequency for the new blade was measured, while it was estimated for the previous blade.

The tracking errors of the new rotor could be held at very low values - in the order of $.2^\circ$ - for advance ratios varying between 0 and 1.0.

Dynamic Rotor Downwash Measurements

Dynamic wake measurements in hovering were made using the single-channel non-linearized hot wire anemometry system available at Washington University.

Figure 1 shows a schematic of the probe arrangement. The probe element was placed .20R below the rotor plane at the .84R blade radius station. The probe was placed so that the radial flow was parallel to the probe wire (therefore radial flow contributed nothing to the probe reading). Thus, the probe registered the sum of the downwash and the tangential flow velocities.

Tangential flow was considered small as compared to the downwash. Justification for this assumption may be obtainable by measurements of the radial and tangential flow components.

Downwash measurements were made for the 2° collective pitch, 3/4 D ground, †1.5° excitation, and $P = 1.20$ case using the Putman Co. manufactured blades, whose dynamic properties are almost identical with the W.U. Manufactured blades. All measurements were made at the same azimuthal position and were recorded on F.M. tape along with the flapping and torsion response. The tape recorded downwash measurements were then analysed on the PDP-12 analog-digital converter and computer using the following scheme.

Let λ equal the downwash measurement and w_f equal the

frequency of excitation in the space fixed reference system.

Then λ_c and λ_s were formed in the following way:

$$\lambda_c = \int_0^{\frac{k2\pi}{\omega_f}} \lambda \cos \omega_f t \quad \text{and} \quad \lambda_s = \int_0^{\frac{k2\pi}{\omega_f}} \lambda \sin \omega_f t$$

where k is the integer necessary to make the quantity

$\left(\frac{k2\pi}{\omega_f}\right)$ an interval over which the excitation is periodic at a

fixed point in space. λ_c , λ_s , and $\sqrt{\lambda_s^2 + \lambda_c^2}$ were calculated

for 7 periods. The means and standard deviations of

$\sqrt{\lambda_s^2 + \lambda_c^2}$ are plotted in Figure 2.

The inaccuracies in the data plotted include:

- 1) The inclusion of tangential flow velocities in the measurements.
- 2) The nonlinearity of the measurement which was not taken into account in the analysis.

The nonlinearity of the measurements was not large enough to seriously effect the description of the dynamic downwash presented in Figure 2.

The measurements of the downwash appear to be reasonably accurate. A full picture of the downwash will require measurements at more radial stations and with more probe positions. For example, aligning the hot wire with the axial direction one will obtain the sum of radial and tangential flow velocity. Based on these preliminary results it was decided that a two-dimensional downwash survey would be profitable. Equipment for such a survey is described in the last section.

Improvements In The Method of Data Processing

The testing effort per test point was cut in half by avoiding testing with 2 different phases of the harmonic input. An algorithm was developed which allowed to obtain all desired results from a single test. This algorithm is described in the section "Analytical Model for Non-Zero Advance Ratio". The previous data processing routine for the PDP-12 computer was completely revised to adapt to the simplified testing procedure and to obtain more output data in reduced time.

The new data processing routine is set up in the following way: At each frequency of excitation 2000 points of the flapping response are gathered at a rate of approximately 36 points per rotor revolution. The time history of the input is defined by 6000 points in order to obtain the precise phase from the phase blips. The response in the rotating system is Fourier analyzed, using Simpson's integration routine, at the frequencies $1 + \omega_f$, $1 - \omega_f$, $2 + \omega_f$, $2 - \omega_f$, $3 + \omega_f$, $3 - \omega_f$, ω_f being the dimensionless frequency in the space fixed system. Furthermore the Fourier components for the frequencies 1 and 2 are obtained. The integration intervals extend from 3 to 7 base periods. A base period is the smallest period consisting of an integer number of both the excitation periods and the periods of rotor revolution. For example, at $\omega_f = .6$ the base period consists of 5 rotor revolutions with approximately 180 points. From the sampling over 3 to 7 base periods mean and standard deviation are determined for all amplitudes, while phase angles are

computed only for the tilting motions. The data processing is performed on the PDP-12 computer using assembly language programs. Analyzing one test run with 13 different excitation frequencies takes about 4.5 hours of computer time.

The program was used in its entirety on data presented in Figures 11a -- 11d and Figures 16a -- 16d which are non-zero advance ratio cases. The standard deviations encountered were so small that a short version of the program was written which did the calculations over only 1 base period thereby shortening the computing time to 1 hour per test run.

Results for successive base period calculations were printed out for a number of data points which showed some deterministic drift in ϕ_{c1} and ϕ_{s1} in some but not all cases printed out. This drift is presumably caused by small rotor speed variations. The maximum amplitude of these drifts was 10 degrees over 7 base periods. At no time has a deterministic drift in $|F_{cn}|$ or $|F_{sn}|$ been observed.

Discussion of Test Results

Figs. 3 to 8 show results for zero advance ratio taken outside the wind tunnel with a ground plate at a distance of $3/4$ rotor diameter from the rotor plane. The flapping response was Fourier analyzed. From the Fourier components corresponding to the excitation frequency, amplitude ratio and phase angle difference were determined. The phase angle scale was shifted upward by 90° , so that for an articulated rotor with cyclic pitch input ($\omega_f = 0$), the phase angle between tip path plane tilt and swashplate tilt is zero. Thus the phase angles shown represent the lag in maximum tip path plane tilt position with respect to the maximum swashplate tilt position. Without dynamic inflow the three amplitude curves shown in Fig. 3 should be identical. The actual difference is an indication of the dynamic inflow effect. The same is true for the phase angles shown in Fig. 4. Since the dynamic inflow should be zero at the flap-bending resonance, one would expect for $P = 1.2$ at $\omega_f = .2$ a zero phase angle. This is approximately true for $\theta_0 = 2^\circ$. The deviations in phase angle from zero at the higher collective pitch settings can be possibly explained by a phase lag of the mean downwash which would produce an in-plane flow component.

In Figs. 5 to 8 the test results for zero advance ratio are compared to the analytical results taken from Eq. 19. The dash lines are for $L = 4$, $\tau = 8$ at collective pitch $\theta_0 = 2^\circ$, and for $L = 2$, $\tau = 4$ at $\theta_0 = 8^\circ$. The solid lines represent

the analysis without dynamic downwash. The measured amplitude ratios correlate very well with the analysis including downwash effects. The measured phase angles are in reasonable agreement with the analysis including dynamic downwash for progressing modes, however there are discrepancies for regressing modes.

Figs. 9 to 16, referring to forward flight are subdivided into 4 sheets each. Sheet (a) shows the absolute value of the time invariable portion of the modulating function $|F_{c0}|$ in comparison with its analytical value (solid line) from Eq. (22). Sheet (a) also shows the measured absolute values of the first and second Fourier components of the trim response with the base frequency Ω . Sheet (b) shows measured and analytical absolute values of the forward tilt ($|F_{c1}|$) and of the left tilt ($|F_{s1}|$), taken from the modulating function Eq. (22). Sheet (c) shows the measured and analytical phase angles of the forward tilting response ϕ_{c1} and of the left tilting response ϕ_{s1} from the modulating function Eq. (22). In case of zero advance ratio shown in Fig. 4 these two curves are identical. Sheet (d) shows the measured and analytical absolute values of the first warping response $|F_{s2}|$ and $|F_{c2}|$ included in the modulating function Eq. (22). The second warping response was also measured but found to be insignificant.

It should be noted again that in Figs. 9 to 16 analytical results shown in solid lines are without dynamic downwash.

Although the tests were conducted with a different rotor model and were evaluated with a different method, the tilting responses at $\mu = .2$ and $\mu = .4$ agree well with the responses presented in Reference 1 including the peculiar double peak of the side tilt amplitude. As the advance ratio is further increased the agreement between test and analytical results becomes better, particularly with respect to tilt response phase angles, although in the vicinity of the blade natural frequency even at $\mu = .8$ substantial deviations are shown, particularly in the side tilt amplitude. The zero and second harmonic of the modulating function show good agreement between test and analytical results, except for the second at high progressing mode frequencies.

The measured trim harmonics are fairly constant over the entire excitation frequency range indicating the absence of substantial non linearities.

Accomplished Work Toward Future Experiments

A. Four Bladed Pitch Stirring Rotor

The four bladed pitch stirring rotor is 90 percent completed. A top and a side view of the rotor are shown in Figures 17 and 18 .

The blades are driven by the hub through extended inner ring micro-precision bearings which allow pitching motion to be transmitted to the blades. The pitching motion is generated by an eccentric rod whose motion is independent of the rotor shaft. The eccentric rod drives, through micro-precision bearings, sets of flexures which transmit a pitching motion to the blades. The amplitude of the motion transmitted is proportional to the eccentricity of the rod. The difference in the eccentric shaft and rotor shaft angular velocities produce progressing or regressing pitching excitations. The eccentric bearings will take a $\pm 3^\circ$ misalignment. At $\pm 1.5^\circ$ excitation the maximum amount of possible play is 3 percent of the total excitation amplitude.

Collective pitch is set by adjusting the relative position of the blade root and the eccentric flexures and then tightening with the adjusting nuts. A detachable collective pitch adjusting plate screws onto the top of the hub. This plate has provisions for holding the collective pitch adjustment rods in position while the nuts are being tightened. Collective pitch can be set precisely by use of a simple optics system utilizing

mirrors on the blade roots, an intense light source, and a ground glass plate.

There exists several possibilities for instrumenting the blades:

- 1) Two blades could be instrumented in the same fashion as the current two bladed rotor and the same single blade analysis could be used to produce rotor response data
- 2) The rotor could be instrumented so that collective coning, differential coning, forward tilt, and left tilt are directly measured. This would require the installation of 4-strain gauges per blade flexure and the installation of resolvers to produce left and forward tilts. A description of the forward and left tilt circuits follows. ± 10 volt 2,400 cps excitation is provided through slip rings to two strain gauge Wheatstone bridges which are wired so that $[\beta_1 + \beta_3]$ and $[\beta_2 + \beta_4]$ are directly produced. These signals go into a resolver placed on the rotor shaft which has 2 rotating coils 90° apart. The resolver also has 2 stationary coils 90° apart so that $\{[\beta_1 + \beta_3]\cos \Omega t + [\beta_2 + \beta_4]\sin \Omega t\}$ and $\{[\beta_1 + \beta_3]\sin \Omega t + [\beta_2 + \beta_4]\cos \Omega t\}$ which are the left and forward tilts, are directly produced. These signals are then sent to AC amplifiers where they are amplified, rectified, and put through a low pass filter so that the carrier frequency is filtered out. Since the signals go through the resolvers

on top of a carrier wave one does not have to worry about phase shifts. Resolvers having the correct properties are available.

Provisions are being made for both kinds of instrumentation, initial tests will use the first kind. For the planned tests with vertically oscillating flow a wind tunnel modification is in progress.

B. Two Dimensional Hovering Wake Survey

A two dimensional hovering wake survey has been planned. The basic measuring device is a hot split film anemometer 2 channel probe. Probe positioning equipment has been designed and built. 1 anemometer channel, 1 signal conditioner, a sum and difference module, and 2 linearizers have been added to the Washington University constant temperature hot wire anemometry equipment so that the two dimensional probe can be utilized. An analog computer will be borrowed to translate the signals coming from the two halves of the probe into orthogonal velocity vectors. The signals will be recorded and later analyzed according to the acheme presented in the section on Dynamic Rotor Downwash Measurements.

Conclusions

1. The improved two bladed rotor model with higher precision blades allowed to measure dynamic flap-bending responses to stirring pitch inputs up to an advance ratio of .8 without encountering any difficulties.
2. Response tests at zero advance ratio correlated reasonably well with an analysis which included dynamic wake effects.
3. The forward flight response tests covered advance ratios .2, .4, .6, .8 at collective pitch settings of 2° and 5° and correlated the better with analytical results without dynamic downwash consideration the higher the advance ratio.
4. Even at .8 advance ratio systematic deviations from the analytical results were observed at low pitch stirring frequencies, indicating dynamic downwash effects extending to high advance ratio.
5. Equipment for dynamic wake measurements has been assembled and spot checked with satisfactory results.
6. A 4 bladed pitch stirring rotor model is almost complete and will be ready for testing in the near future.

References

1. Hohenemser, K. H. and Crews, S. T., "Experiments with Progressing/Regressing Forced Rotor Flapping Modes", Phase VI-B Report under Contract NAS2-4151, June 1972.
2. Hohenemser, K. H. and Crews, S. T., "Unsteady Wake Effects on Progressing/Regressing Forced Rotor Flapping Modes", AIAA 2nd Atmospheric Flight Mechanics Conference, Palo Alto, California, September 1972, AIAA Paper No. 72-957.
3. Hohenemser, K. H. and Crews, S. T., "Model Tests on Unsteady Rotor Wake Effects", Journal of Aircraft, Vol. 10 No. 1, January 1973, pp. 58-60.
4. Carpenter, P. J. and Fridovich, B., "Effects of a Rapid Blade Pitch Increase on the Thrust and Induced Velocity Response of a Full Scale Helicopter Rotor NACA TN 3044, November 1953.
5. Hohenemser, K. H. and Yin, S. K., "Some Applications of the Method of Multiblade Coordinates", Journal American Helicopter Society, Vol. 17, No. 3, July 1972.
6. Hohenemser, K. H. and Yin, S. K., "Flap Bending Corrections to the Rigid Blade Analysis of Lifting Rotors", Phase VI-A Report under Contract NAS2-4151, Part II, June 1972.

Figure Captions

Fig. 1	Probe Location for Wake Survey
Fig. 2	Measured Wake Amplitudes
Fig. 3	Measured Amplitude Ratio vs. Frequency for 3 Collective Pitch Values
Fig. 4	Measured Phase Angle vs. Frequency for 3 Collective Pitch Values
Fig. 5	Amplitude Ratio, $\theta_0 = 2^\circ$, $\mu = 0$
Fig. 6	Amplitude Ratio, $\theta_0 = 8^\circ$, $\mu = 0$
Fig. 7	Phase Angle, $\theta_0 = 2^\circ$, $\mu = 0$
Fig. 8	Phase Angle, $\theta_0 = 8^\circ$, $\mu = 0$
Fig. 9 a-d	Fourier Coefficients and Phase Angles, $P = 1.2$, $\theta_0 = 2^\circ$, $\mu = .2$
Fig. 10 a-d	Fourier Coefficients and Phase Angles, $P = 1.2$, $\theta_0 = 5^\circ$, $\mu = .2$
Fig. 11 a-d	Fourier Coefficients and Phase Angles, $P = 1.10$, $\theta_0 = 5^\circ$, $\mu = .2$
Fig. 12 a-d	Fourier Coefficients and Phase Angles, $P = 1.20$, $\theta_0 = 2^\circ$, $\mu = .4$
Fig. 13 a-d	Fourier Coefficients and Phase Angles, $P = 1.20$, $\theta_0 = 5^\circ$, $\mu = .4$
Fig. 14 a-d	Fourier Coefficients and Phase Angles, $P = 1.10$, $\theta_0 = 5^\circ$, $\mu = .4$
Fig. 15 a-d	Fourier Coefficients and Phase Angles, $P = 1.20$, $\theta_0 = 2^\circ$, $\mu = .6$
Fig. 16 a-d	Fourier Coefficients and Phase Angles, $P = 1.20$, $\theta_0 = 2^\circ$, $\mu = .8$
Fig. 17	Side View, Pitch Stirring Rotor
Fig. 18	Top View, Pitch Stirring Rotor

Figure 1 Rotor-Probe Schematic

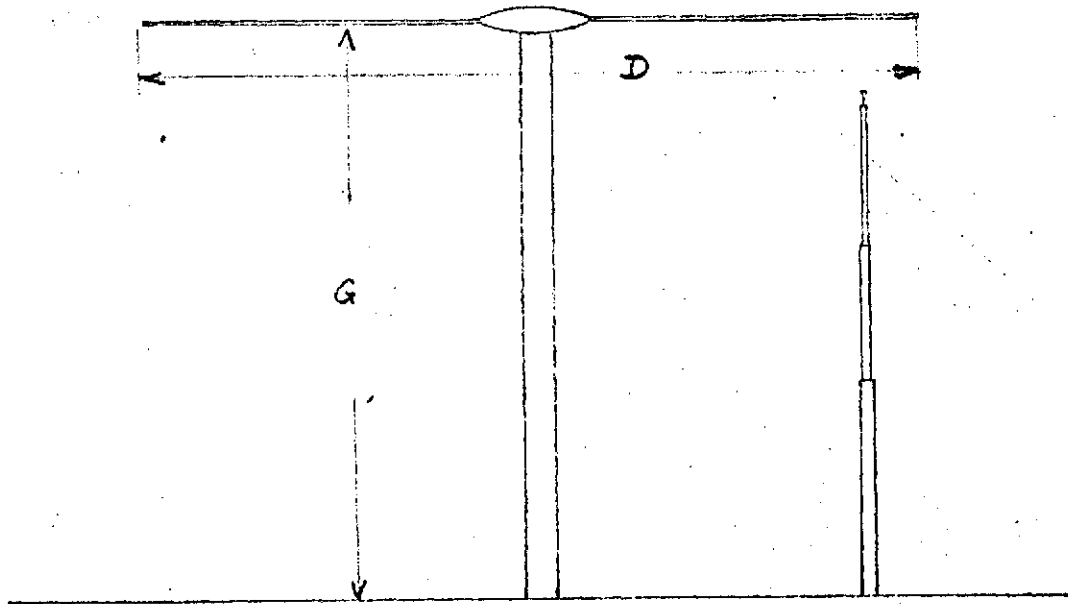


Figure 2 Dynamic Wake Measurements

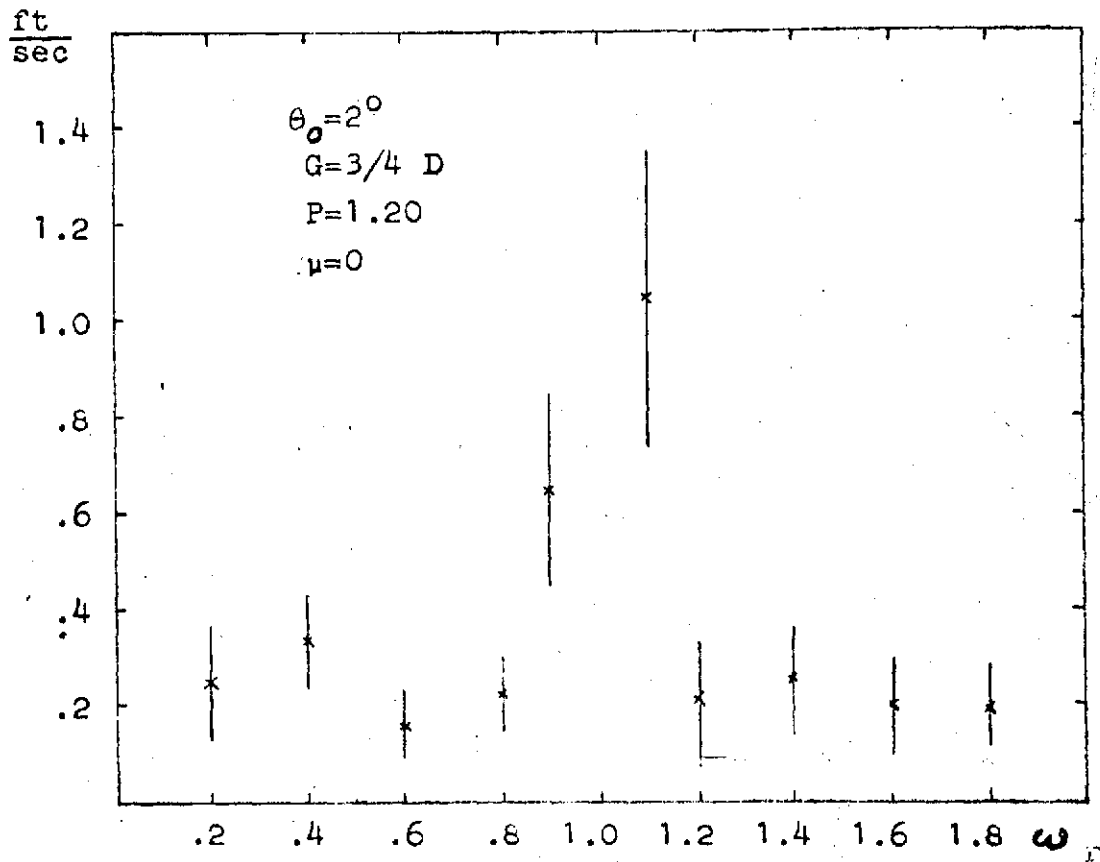


Figure 3
 $G=3/4D$

- ——— $\theta_0 = 2^\circ$
- - - - $\theta_0 = 5^\circ$
- x - - - $\theta_0 = 8^\circ$

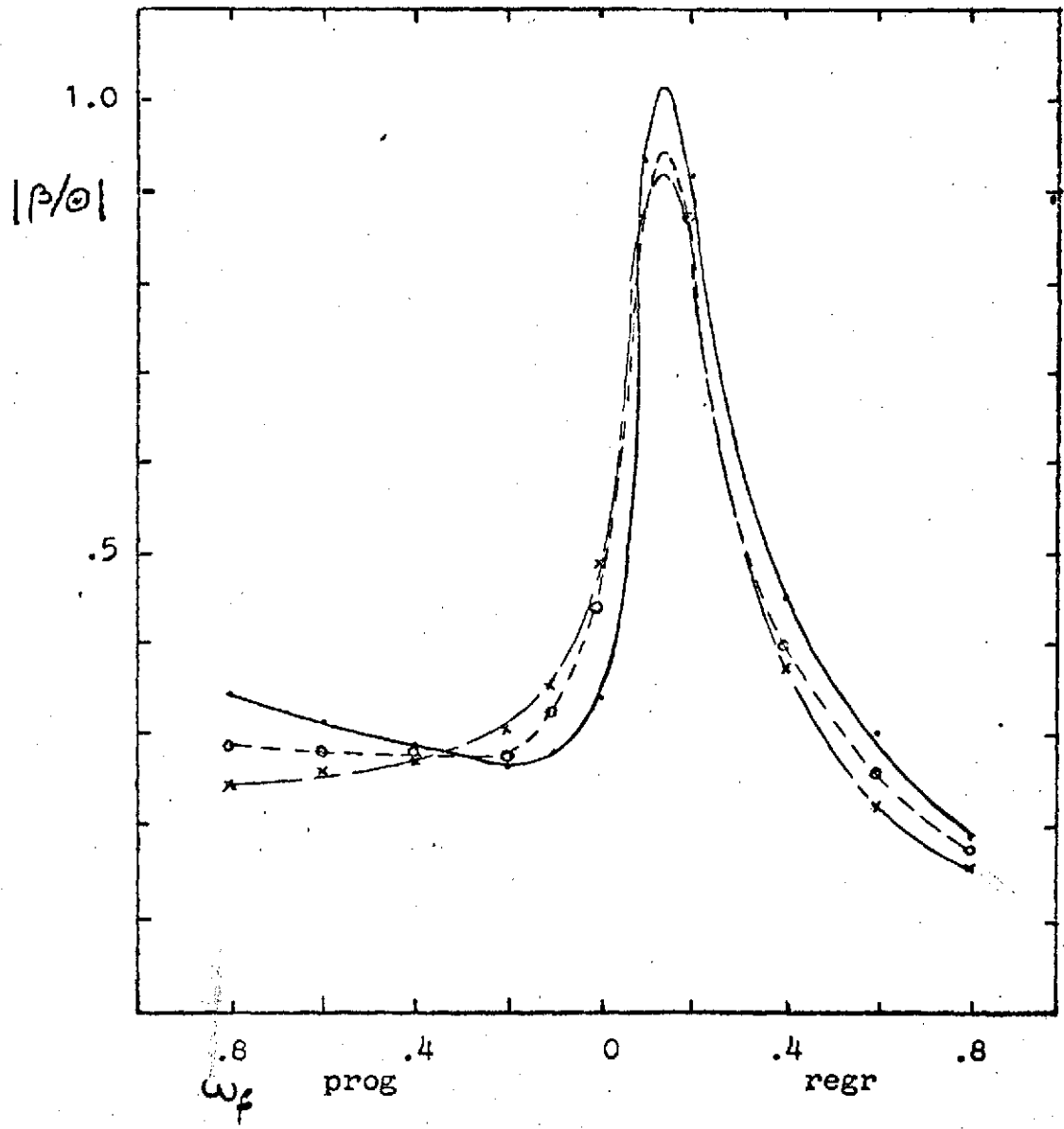
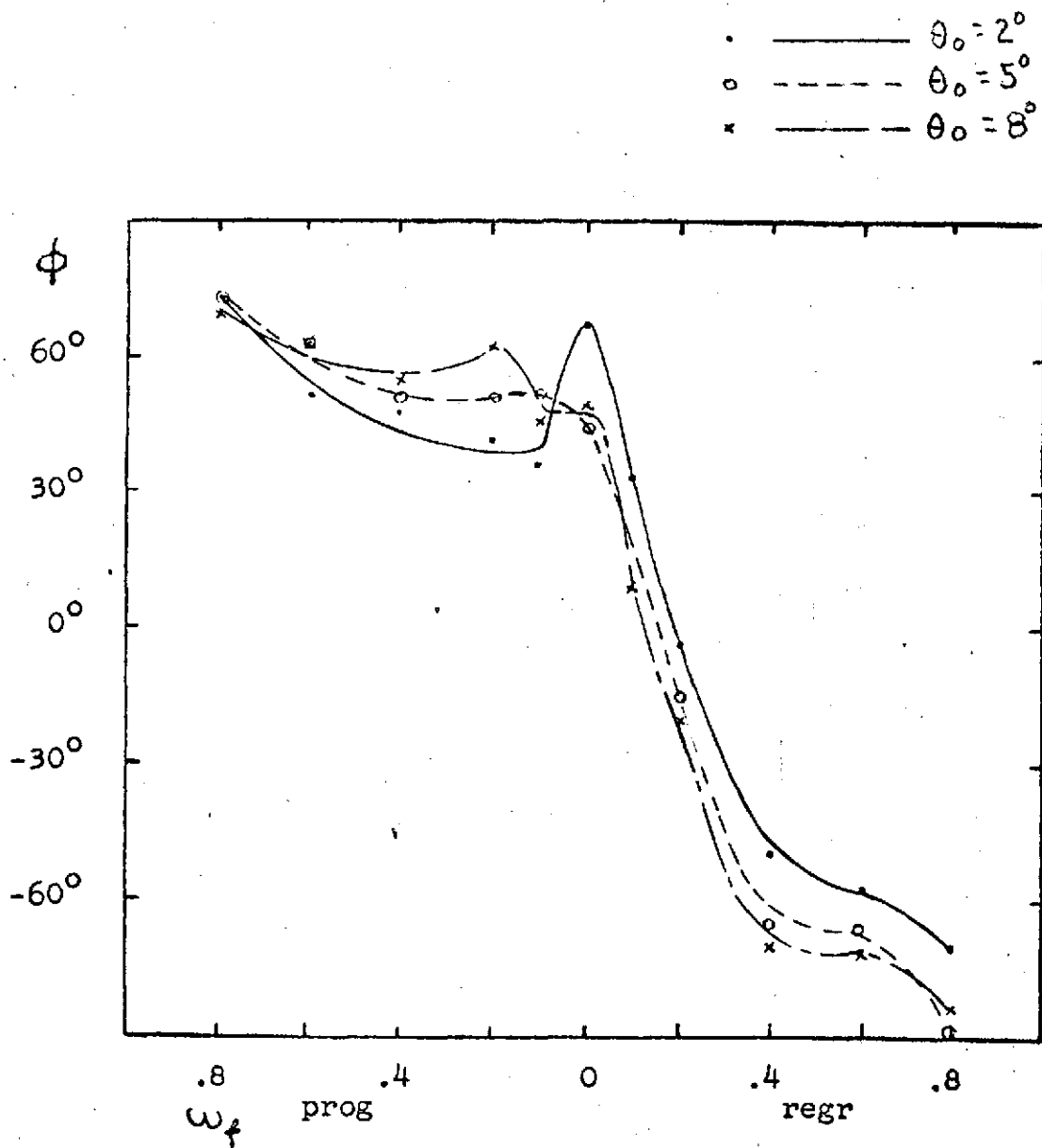


Figure 4
 $G=3/4D$



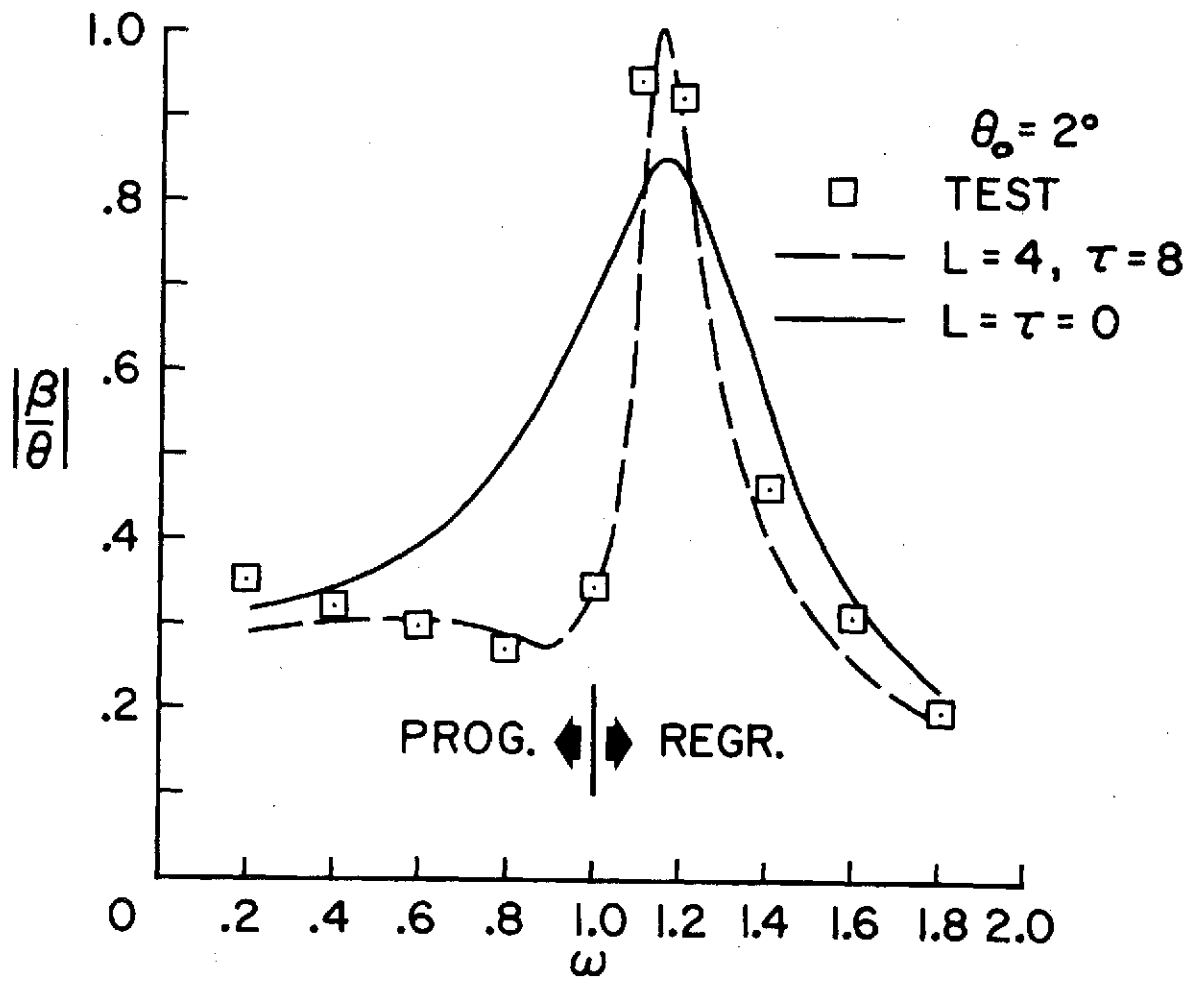


Fig. 5

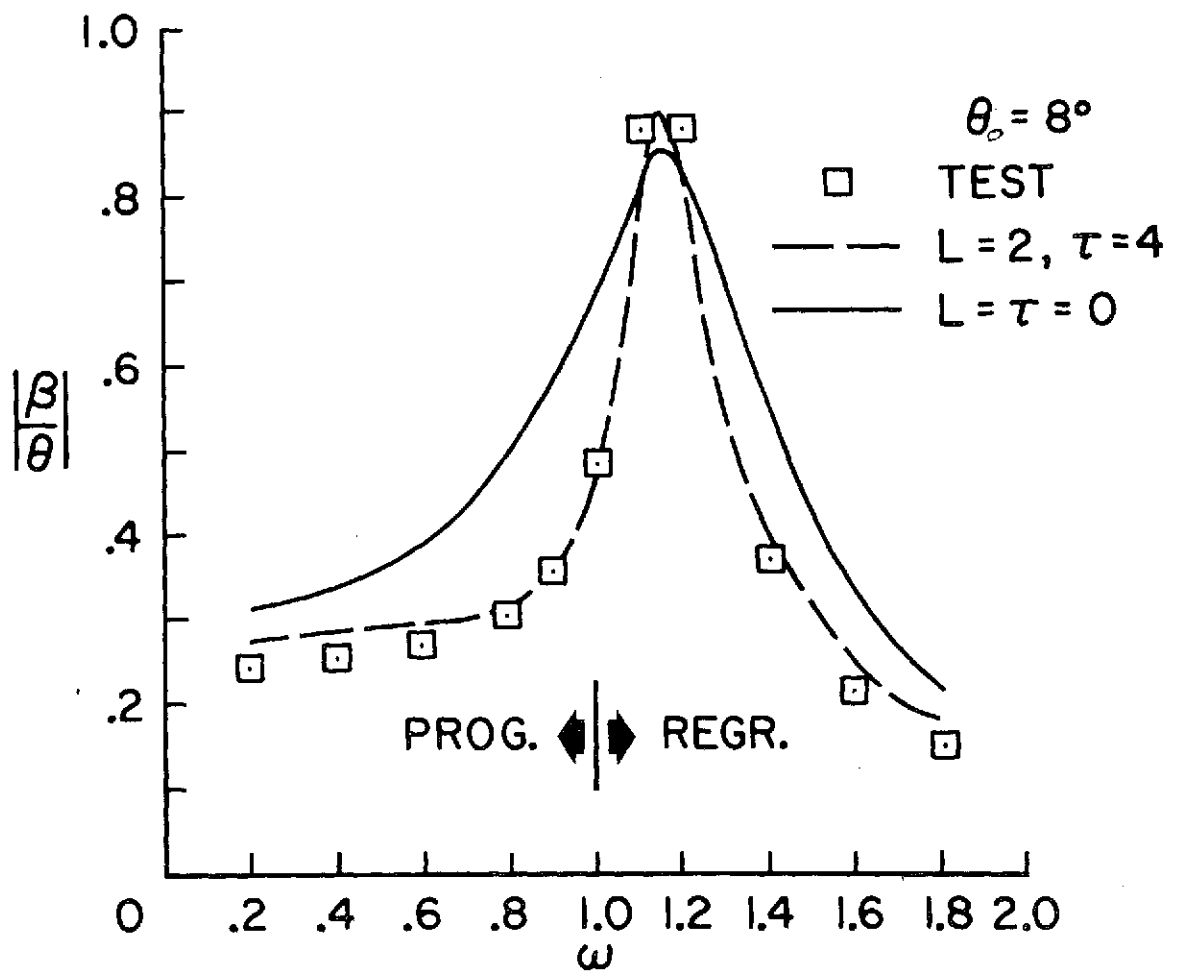


FIG. 6

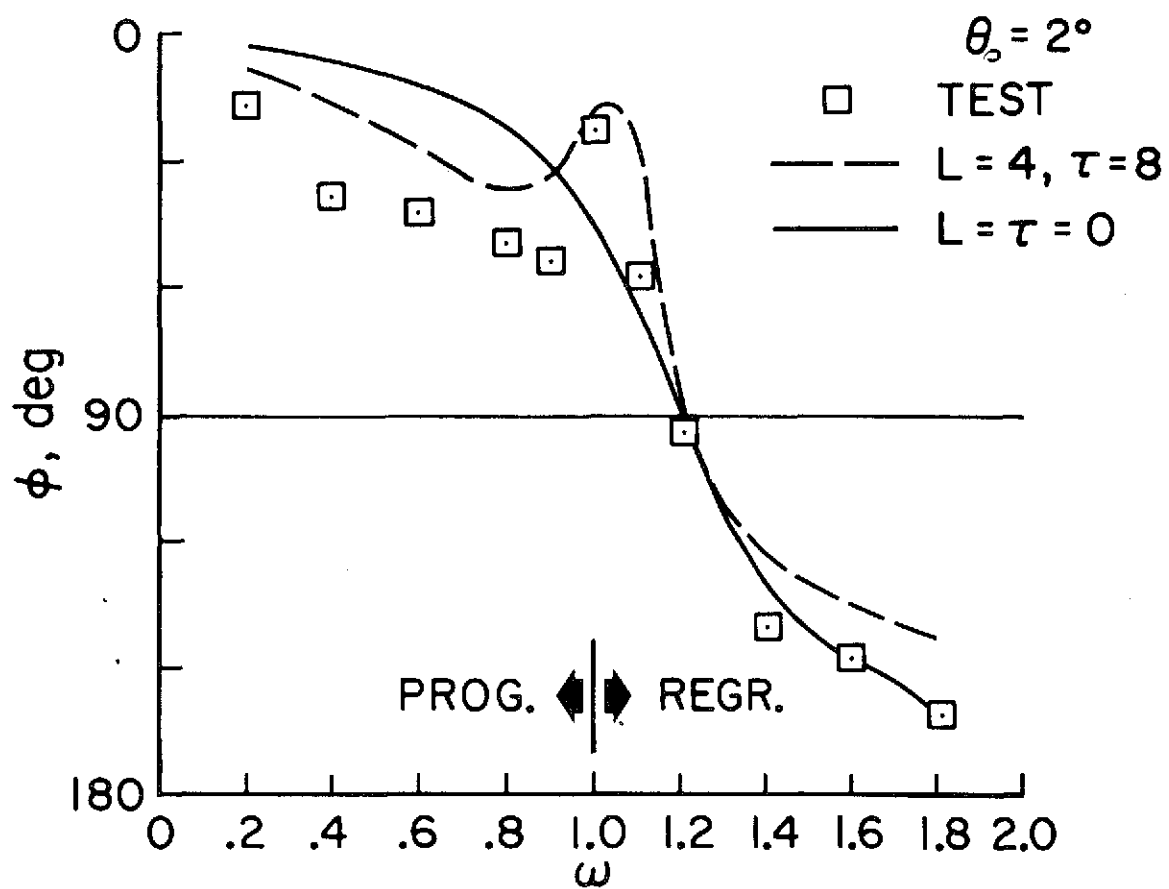


Fig. 7

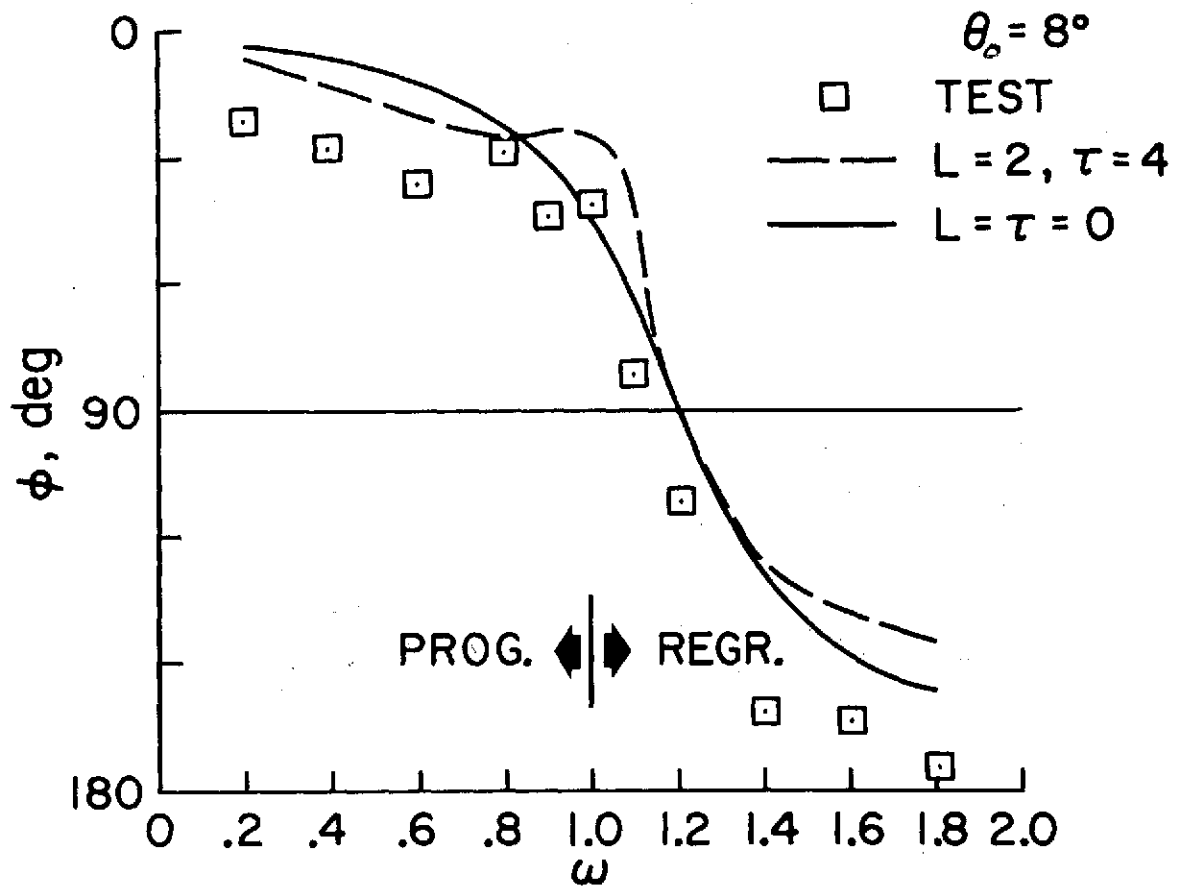


Fig. 8

$\mu = .2$
 $P = 1.20$
 $\theta_0 = 2^\circ$
 $\theta_c = \pm 1.5^\circ$

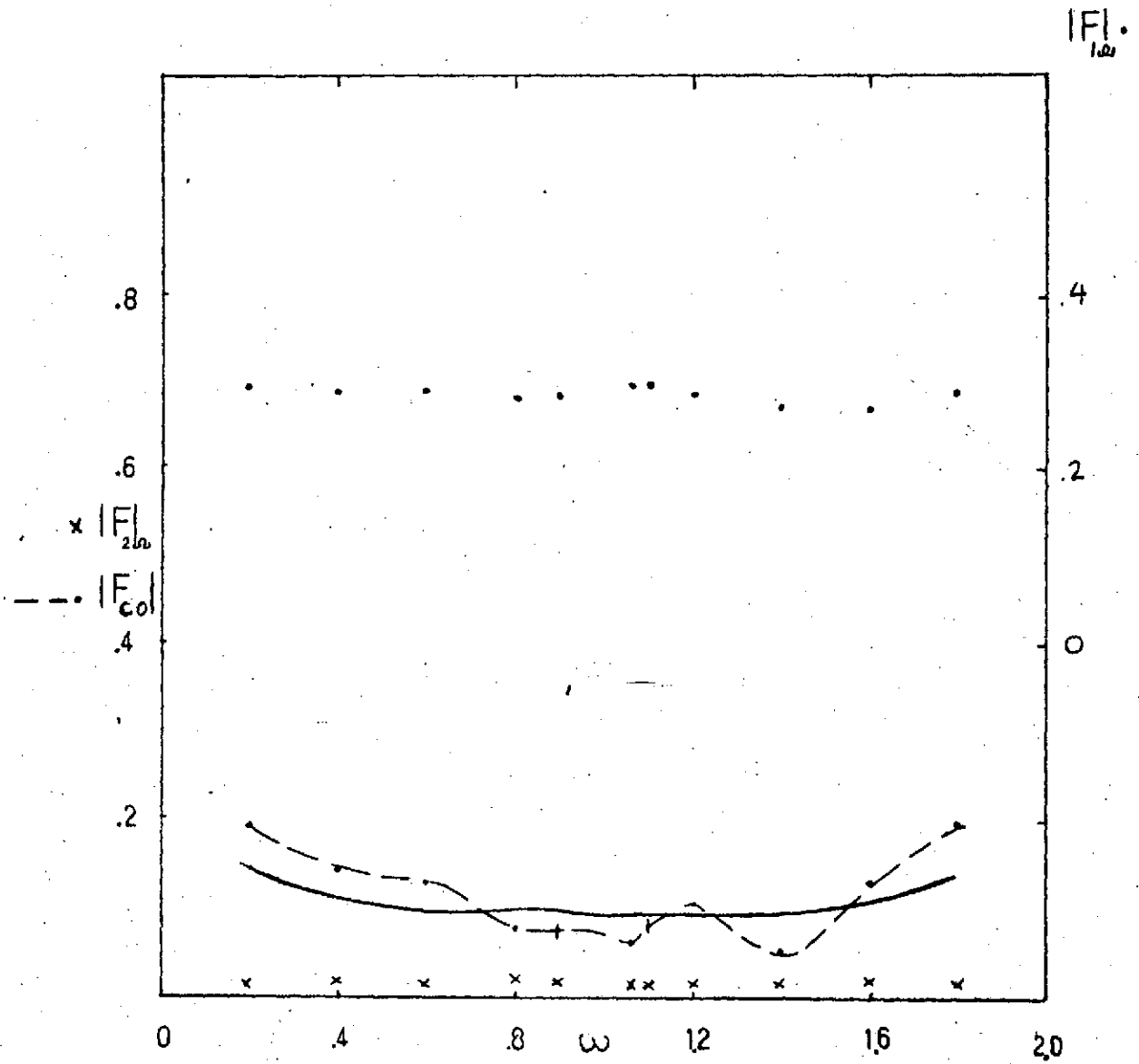


Fig. 9a

$\mu = .2$
 $P = 1.20$
 $\theta_0 = 2^\circ$
 $\theta_c = \pm 1.5^\circ$

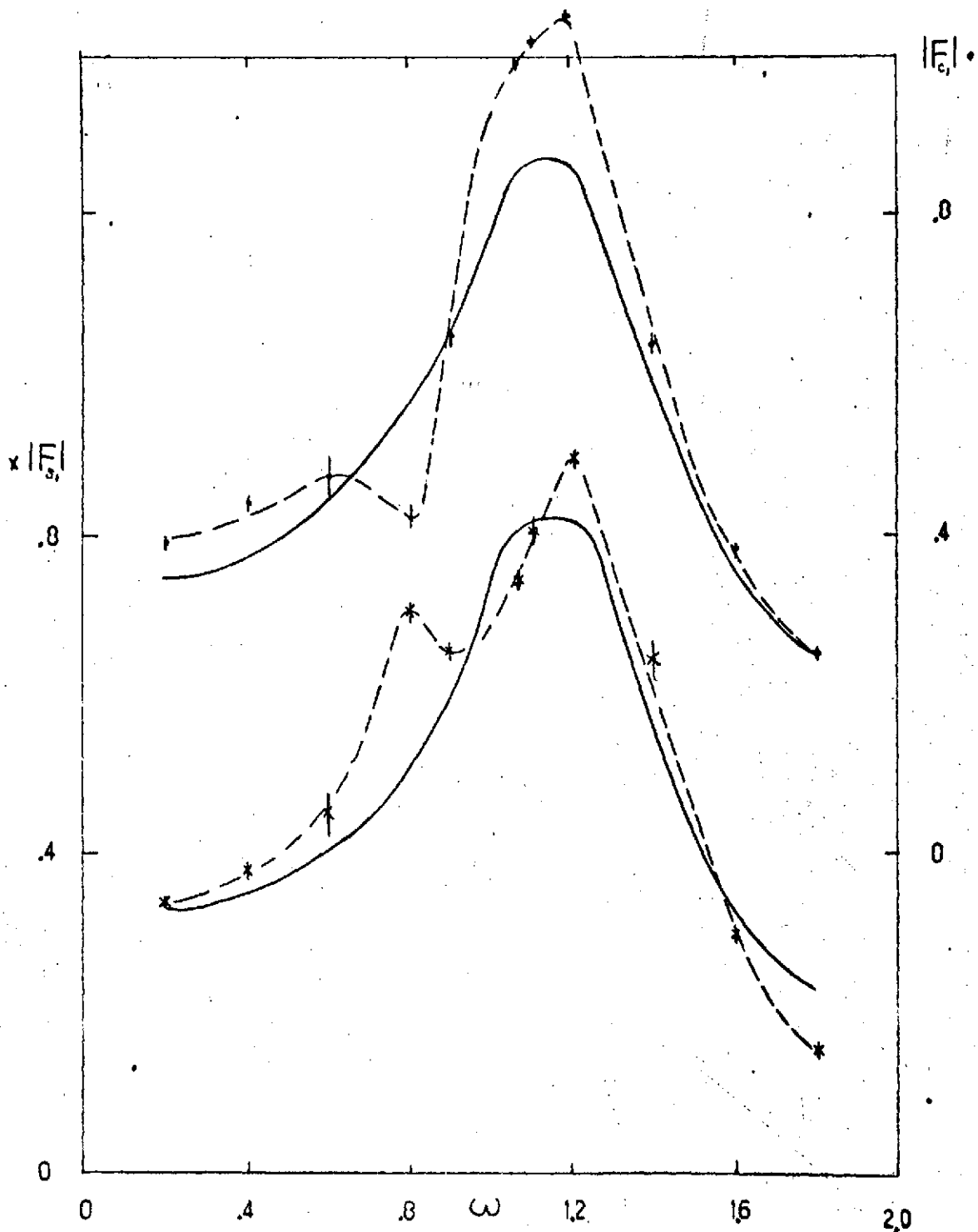


Fig. 9b

$$\mu = .2$$

$$P = 1.20$$

$$\theta_0 = 2^\circ$$

$$\theta_c = \pm 1.5$$

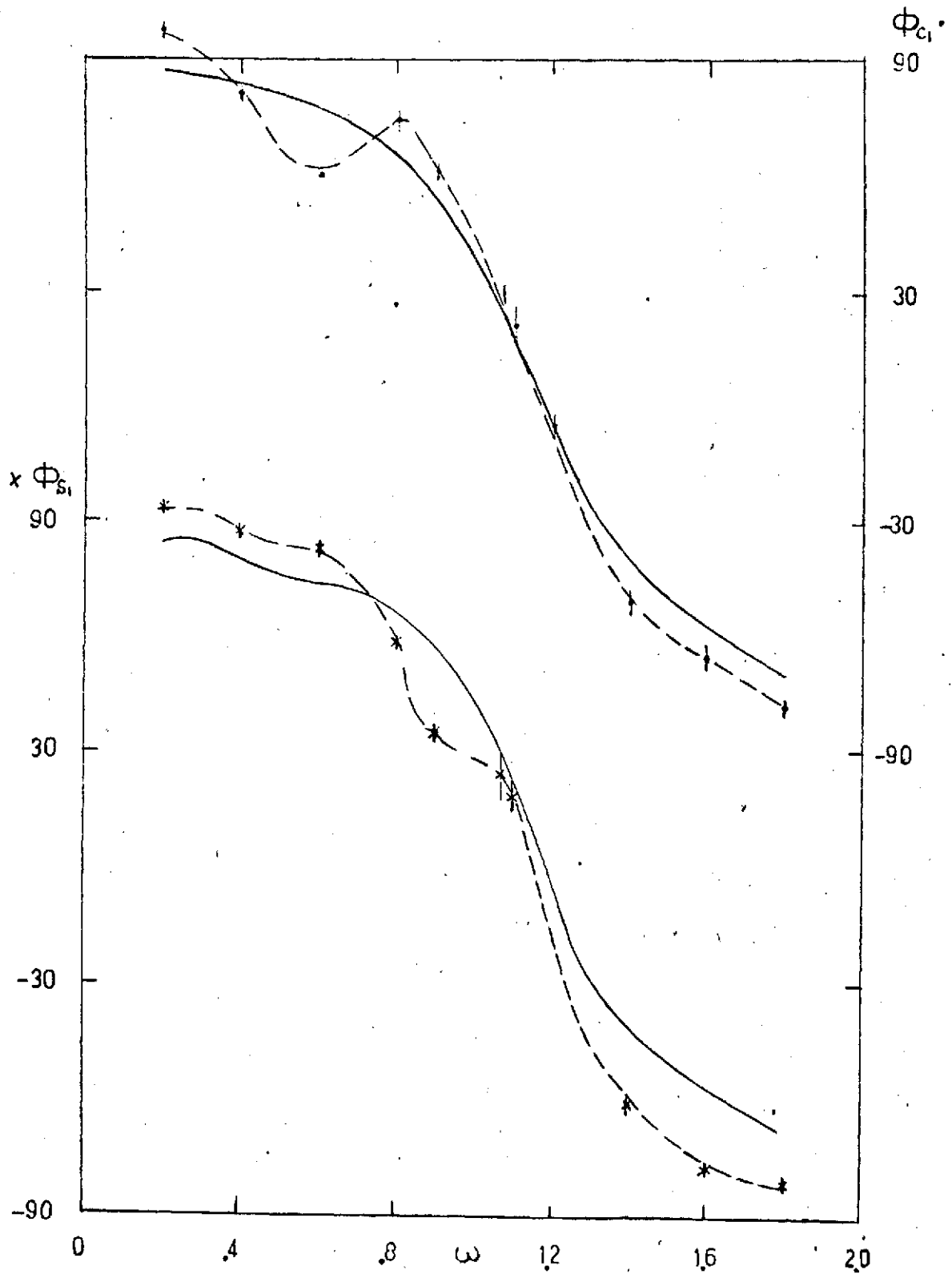


Fig. 9c

$\mu = .2$
 $P = 1.20$
 $\theta_0 = 2^\circ$
 $\theta_c = \pm 1.5$

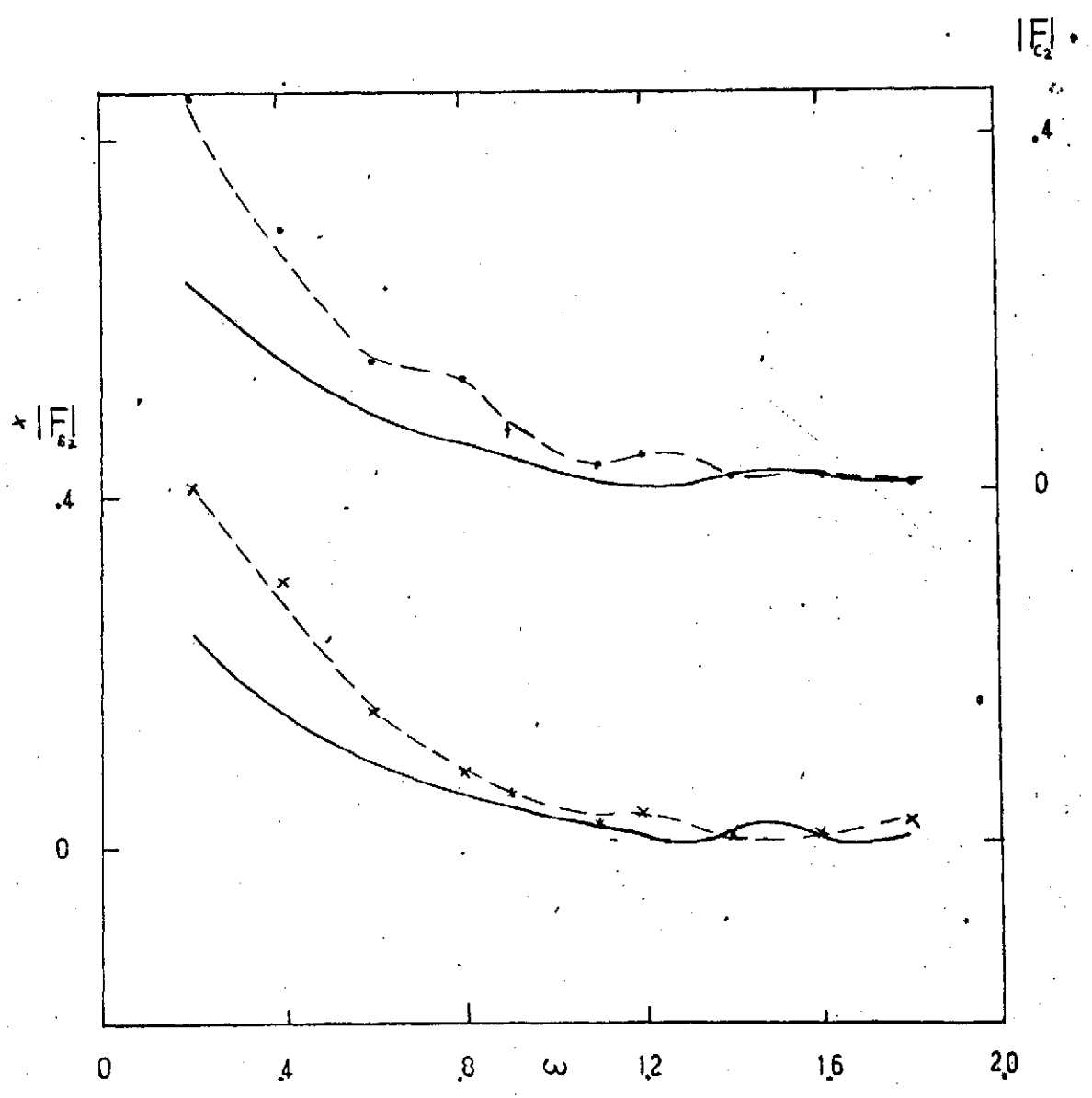


Fig. 9d

$$\mu = .2$$

$$P = 1.20$$

$$\theta_0 = 5^\circ$$

$$\theta_{cyc} = \pm 1.5^\circ$$

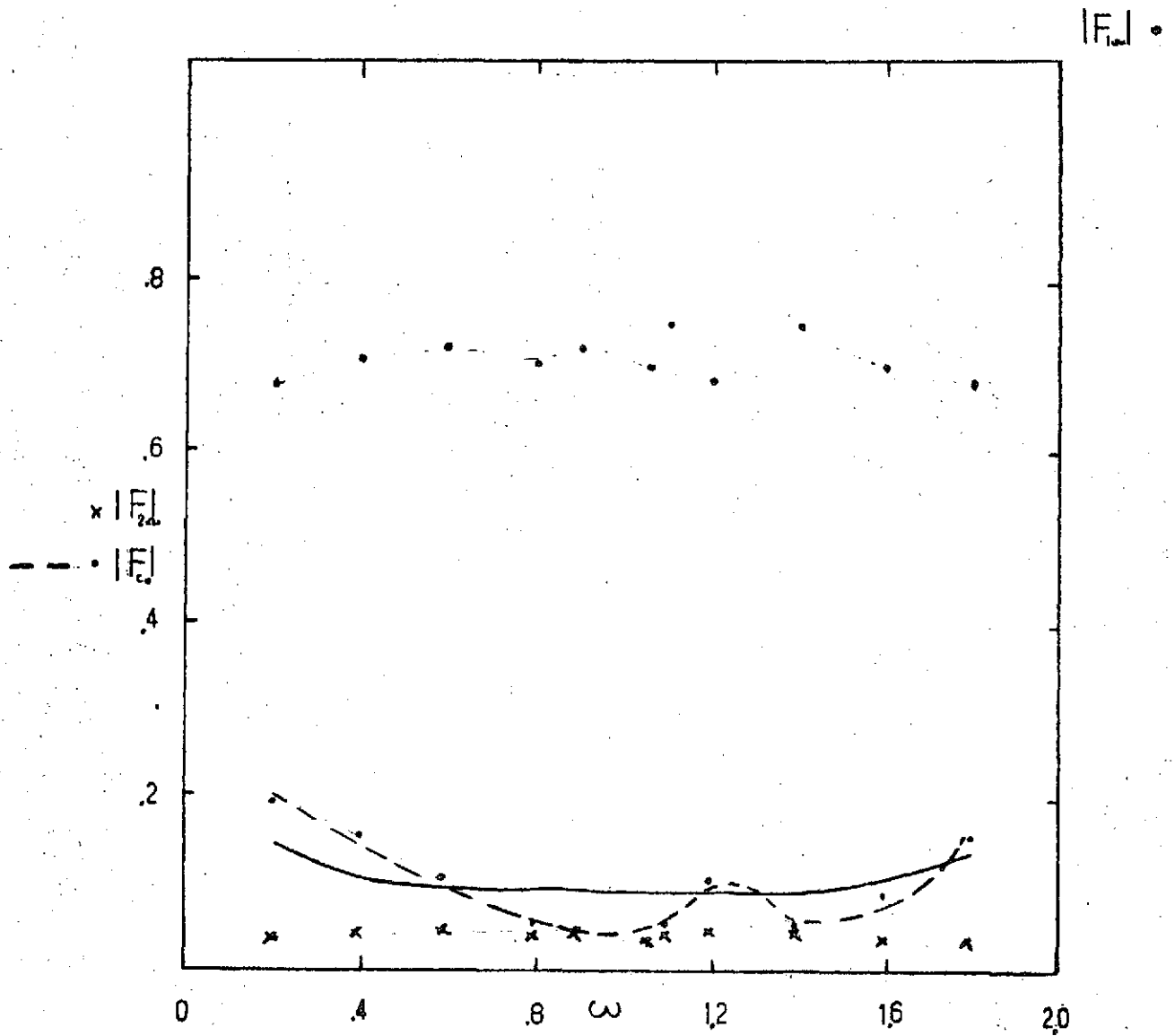


Fig. 10a

$$\mu = .2$$

$$P = 1.20$$

$$\theta_0 = 5^\circ$$

$$\theta_{cyc} = \pm 1.5^\circ$$

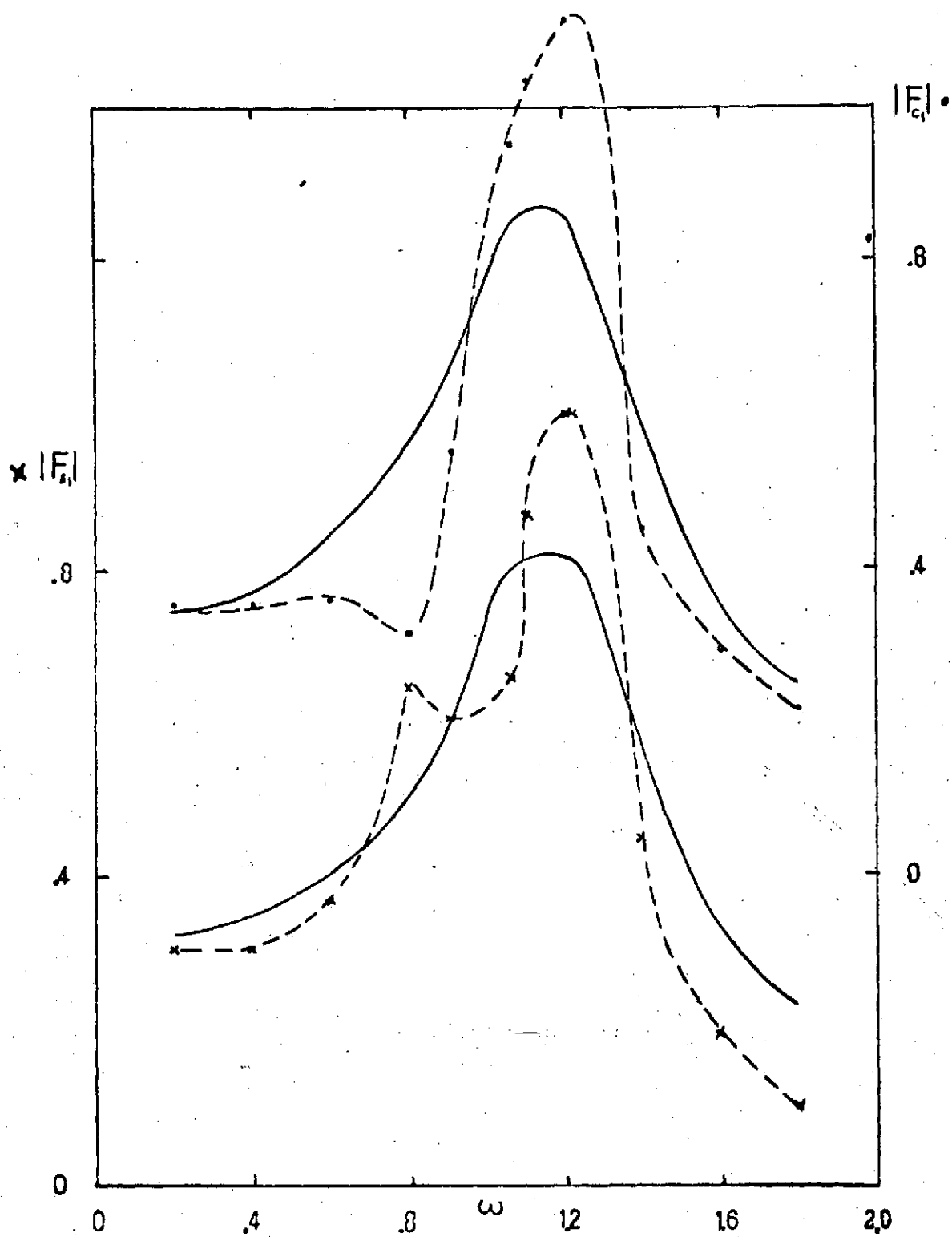


Fig. 10b

$$\begin{aligned} \nu &= .2 \\ P &= 1.20 \\ \theta_0 &= 5^\circ \\ \theta_c &= \pm 1.5^\circ \end{aligned}$$

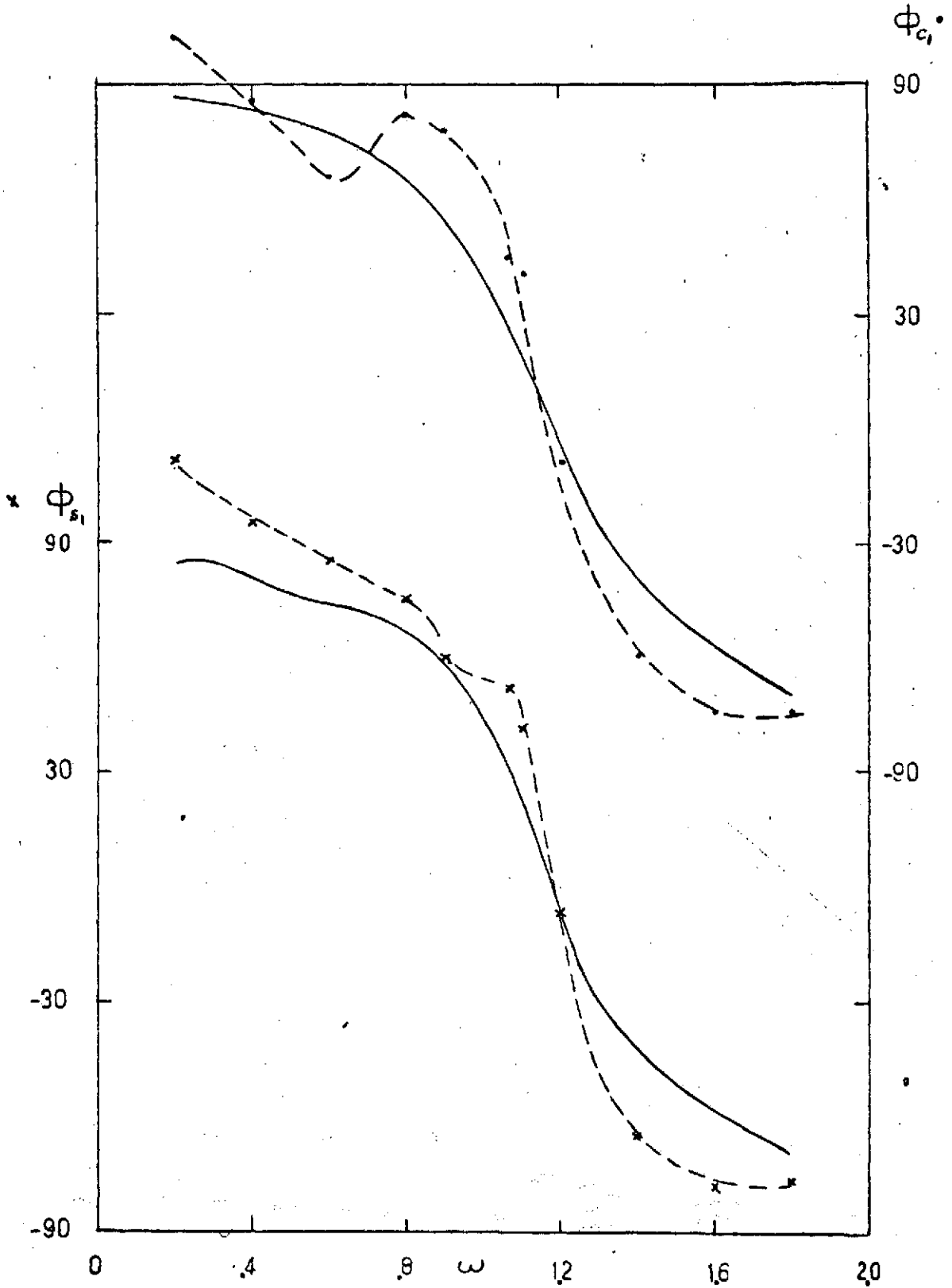


Fig. 10c

$\mu = .2$
 $P = 1.20$
 $\theta_0 = 5^\circ$
 $\theta_c = \pm 1.5^\circ$

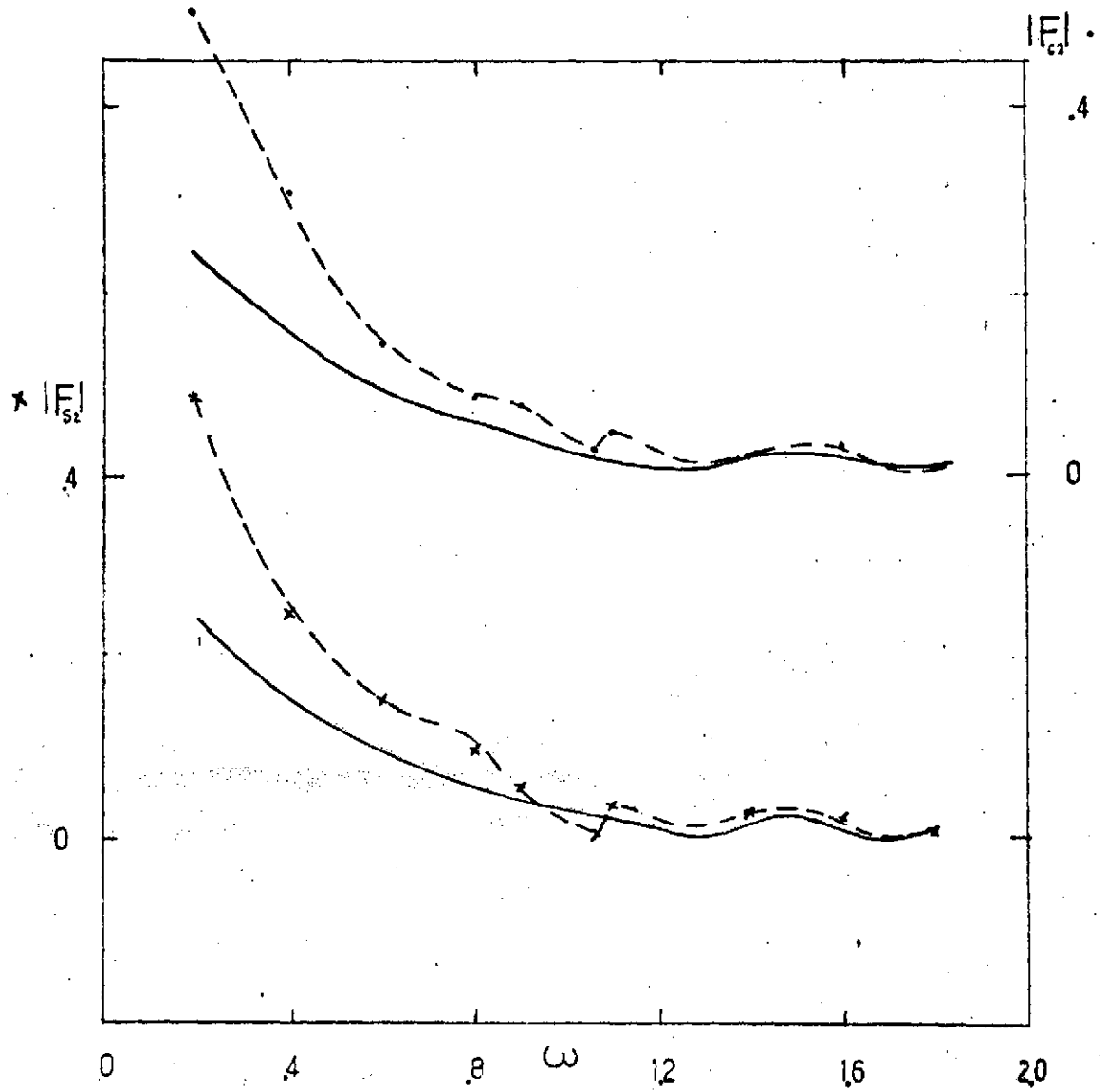


Fig.10d

$\mu = .2$
 $P = 1.10$
 $\theta_0 = 5^\circ$
 $\theta_c = \pm 1.5$

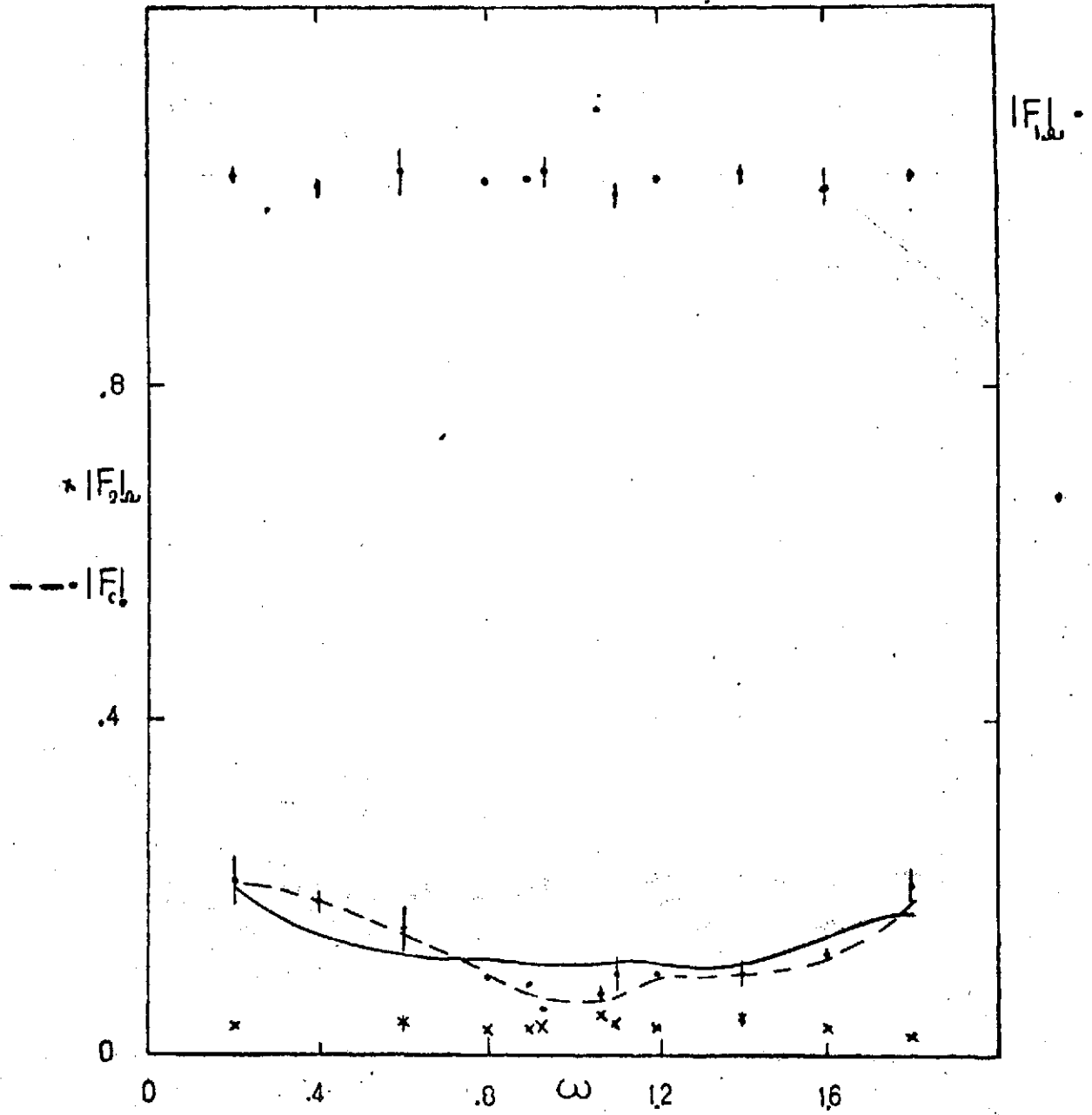


Fig. 11a

$\nu = .2$
 $P = 1.10$
 $\theta_0 = 5^\circ$
 $\theta_c = \pm 1.0$

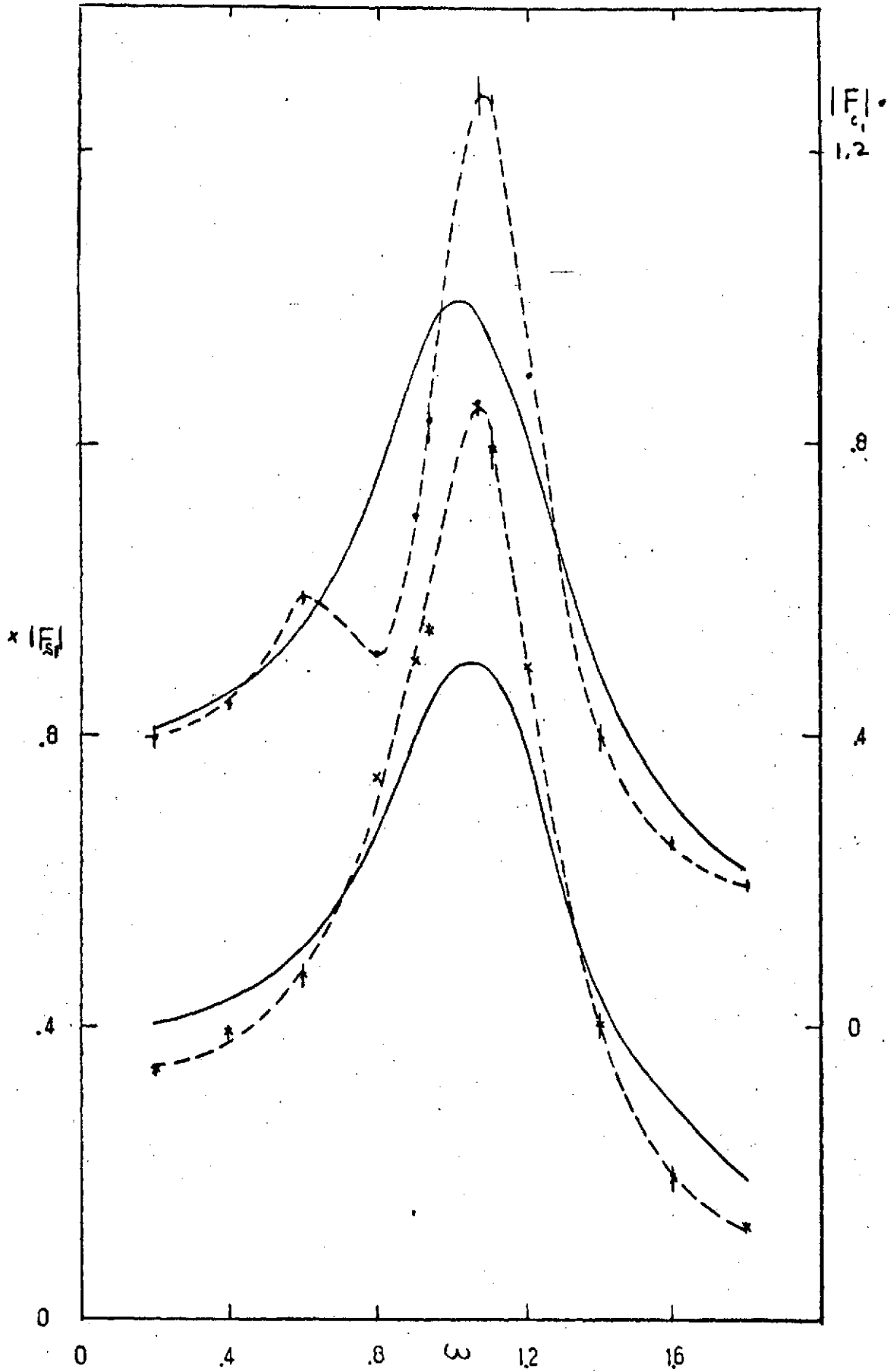


FIG. 11b

$$\begin{aligned} \mu &= .2 \\ P &= 1.1 \\ \theta_0 &= 5^\circ \\ \theta_c &= \pm 1.5^\circ \end{aligned}$$

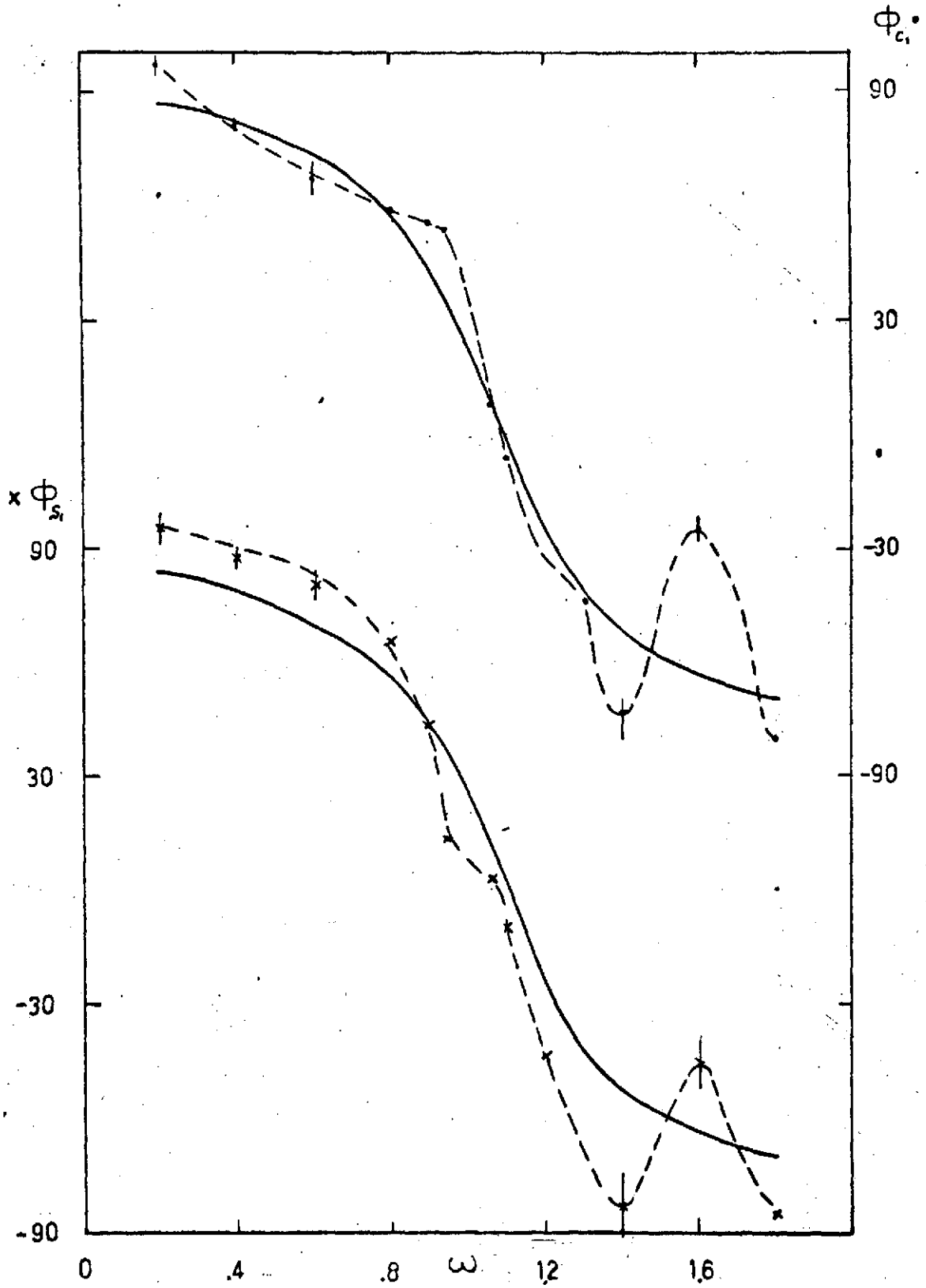


Fig. 11c

$\mu = .2$
 $P = 1.10$

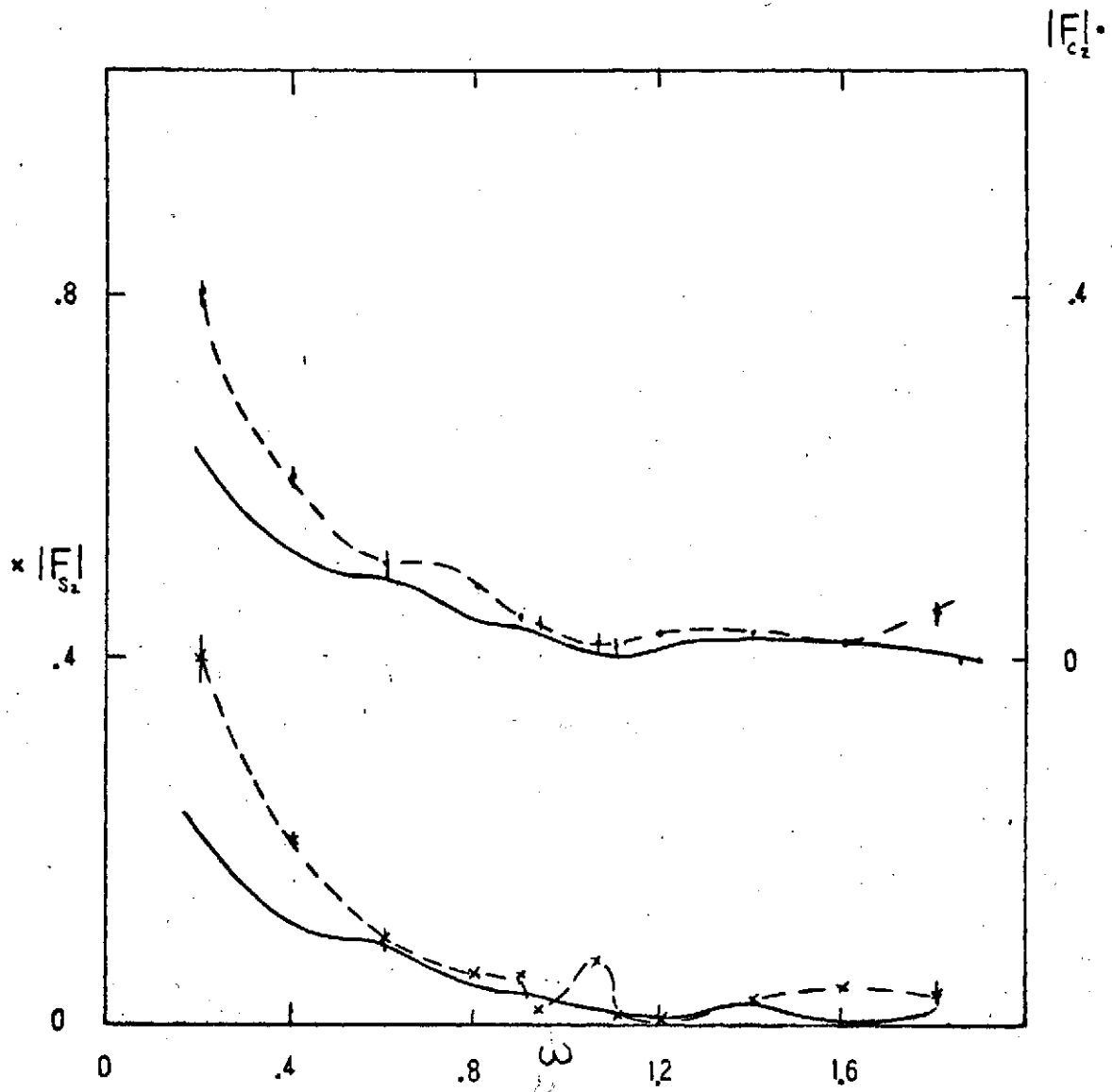
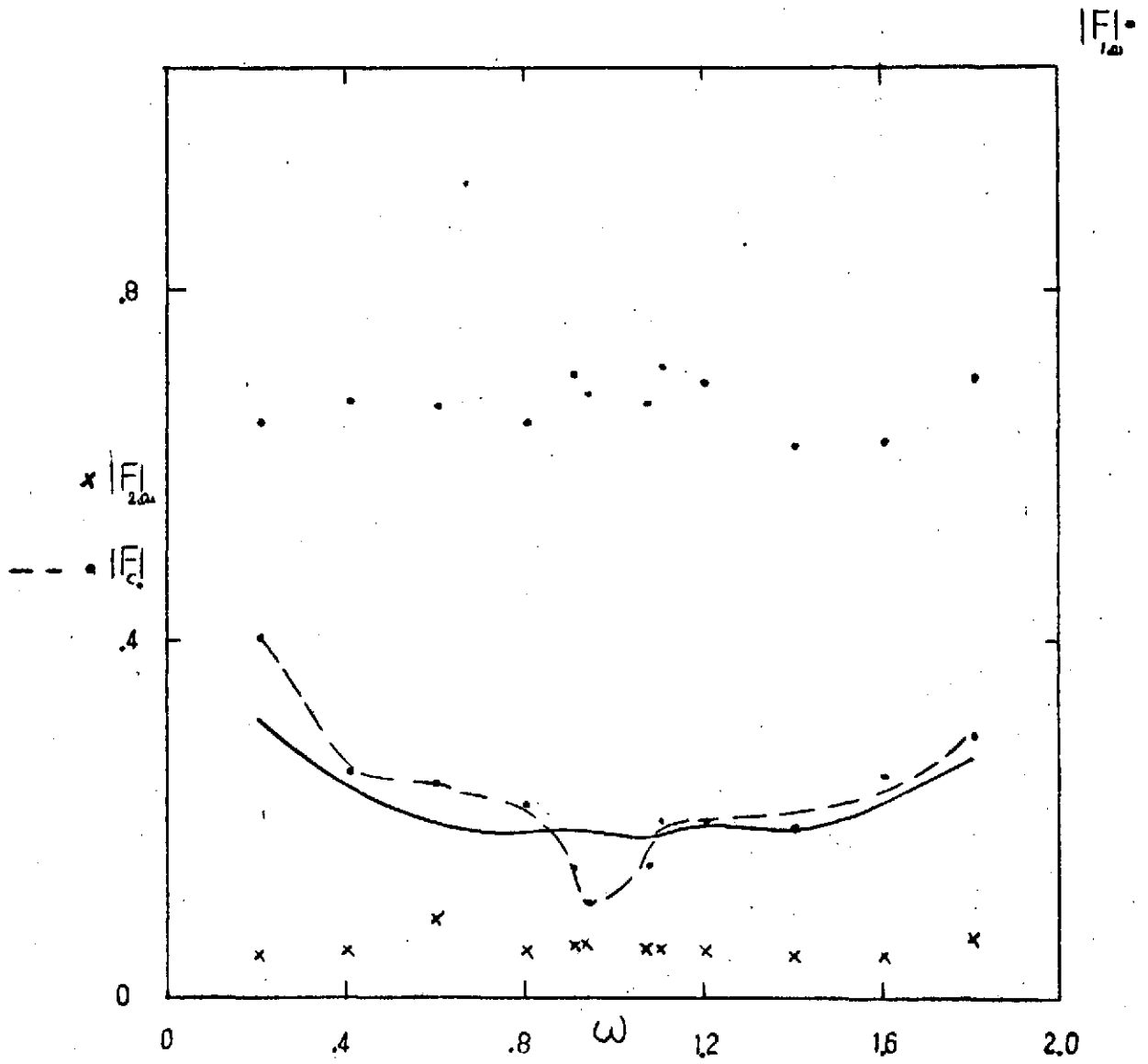


Fig. 11d

$\mu = .4$
 $P = 1.20$
 $\theta_0 = 2^\circ$
 $\theta_c = \pm 1.5^\circ$



$\nu = .4$
 $P = 1.20$
 $\theta_0 = 2^\circ$
 $\theta_c = \pm 1.5^\circ$

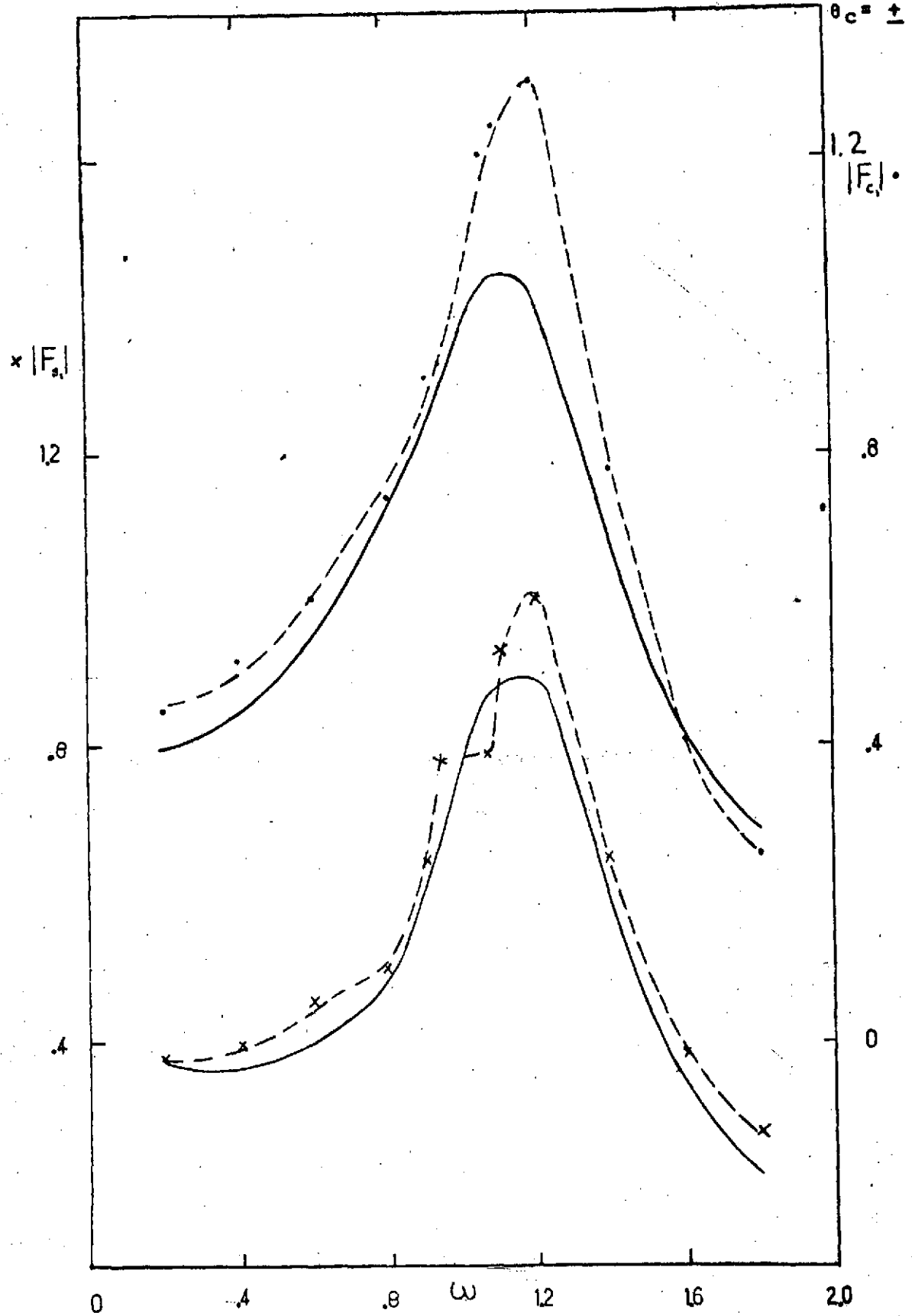


Fig. 12b

$$\begin{aligned} \mu &= .4 \\ P &= 1.20 \\ \theta_o &= 2^\circ \\ \theta_c &= \pm 1.5^\circ \end{aligned}$$

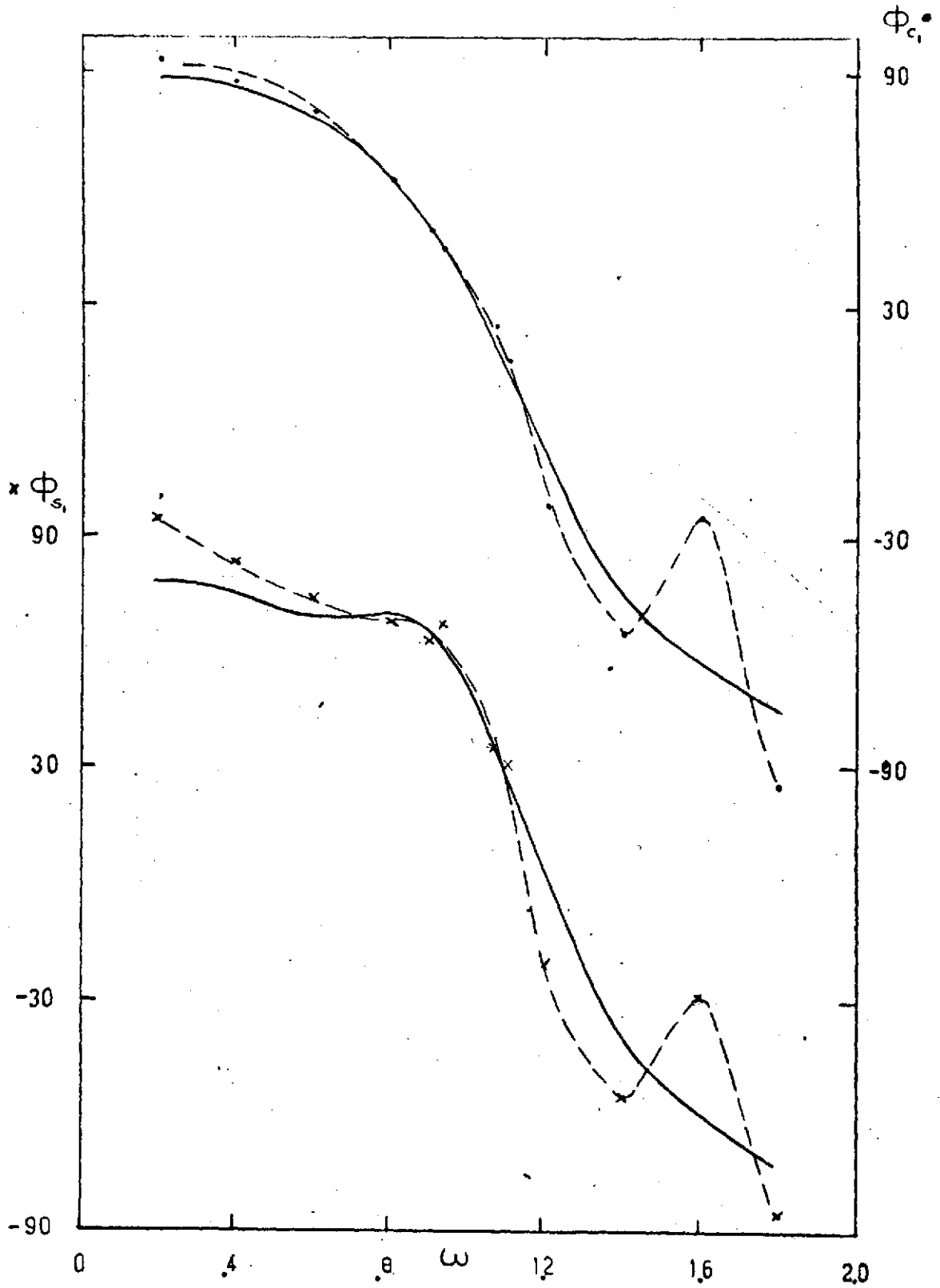


Fig. 12c

$\mu = .4$
 $P = 1.20$
 $\theta_0 = 2^\circ$
 $\theta_c = \pm 1.5^\circ$

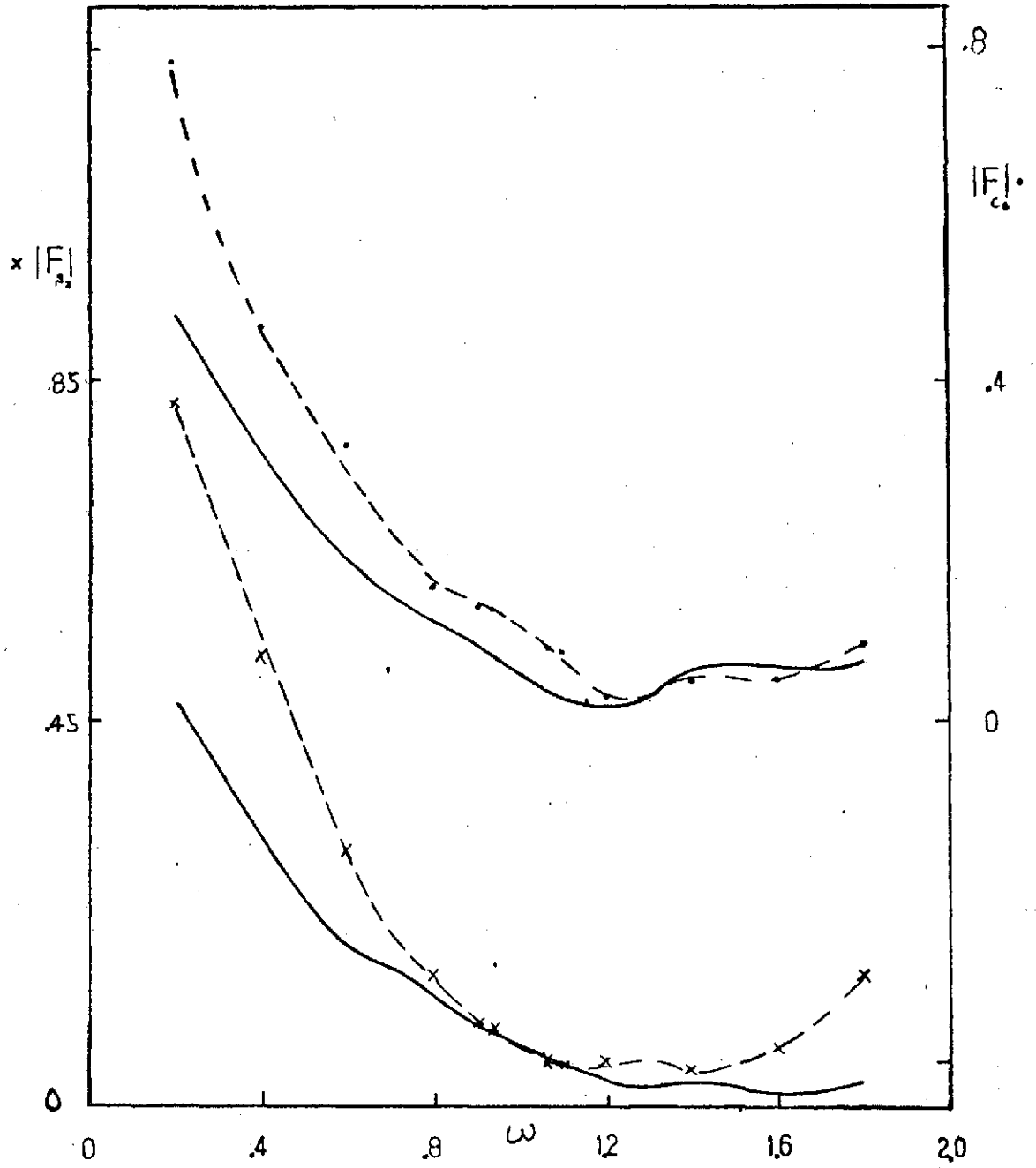


Fig. 12d

$\mu = .4$
 $P = 1.20$
 $\theta_0 = 5^\circ$
 $\theta_{cyc} = \pm 1.5^\circ$

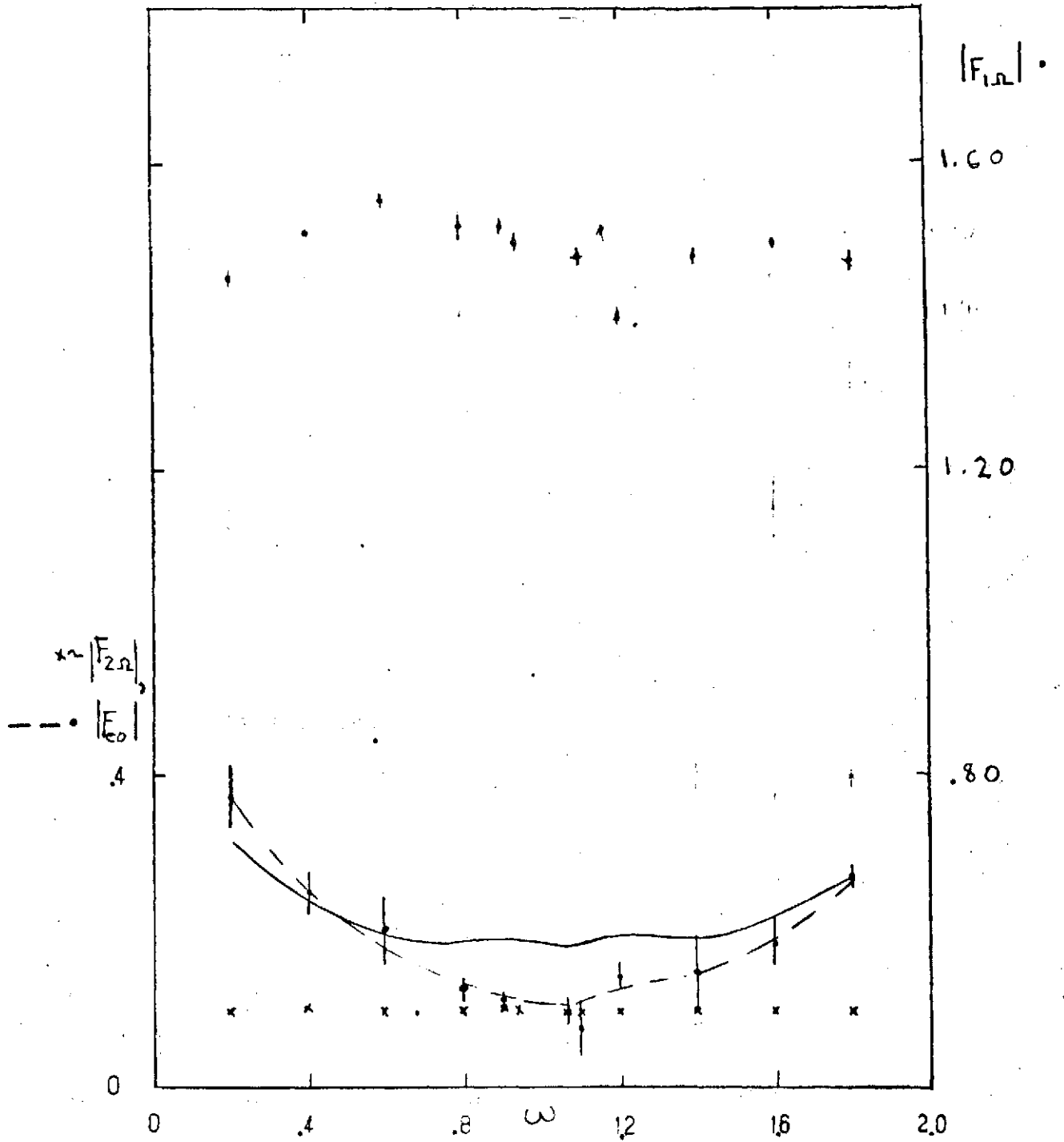


Fig. 13a

$\mu = .4$
 $P = 1.20$
 $\theta_0 = 5^\circ$
 $\theta_{cyc} = \pm 1.5^\circ$

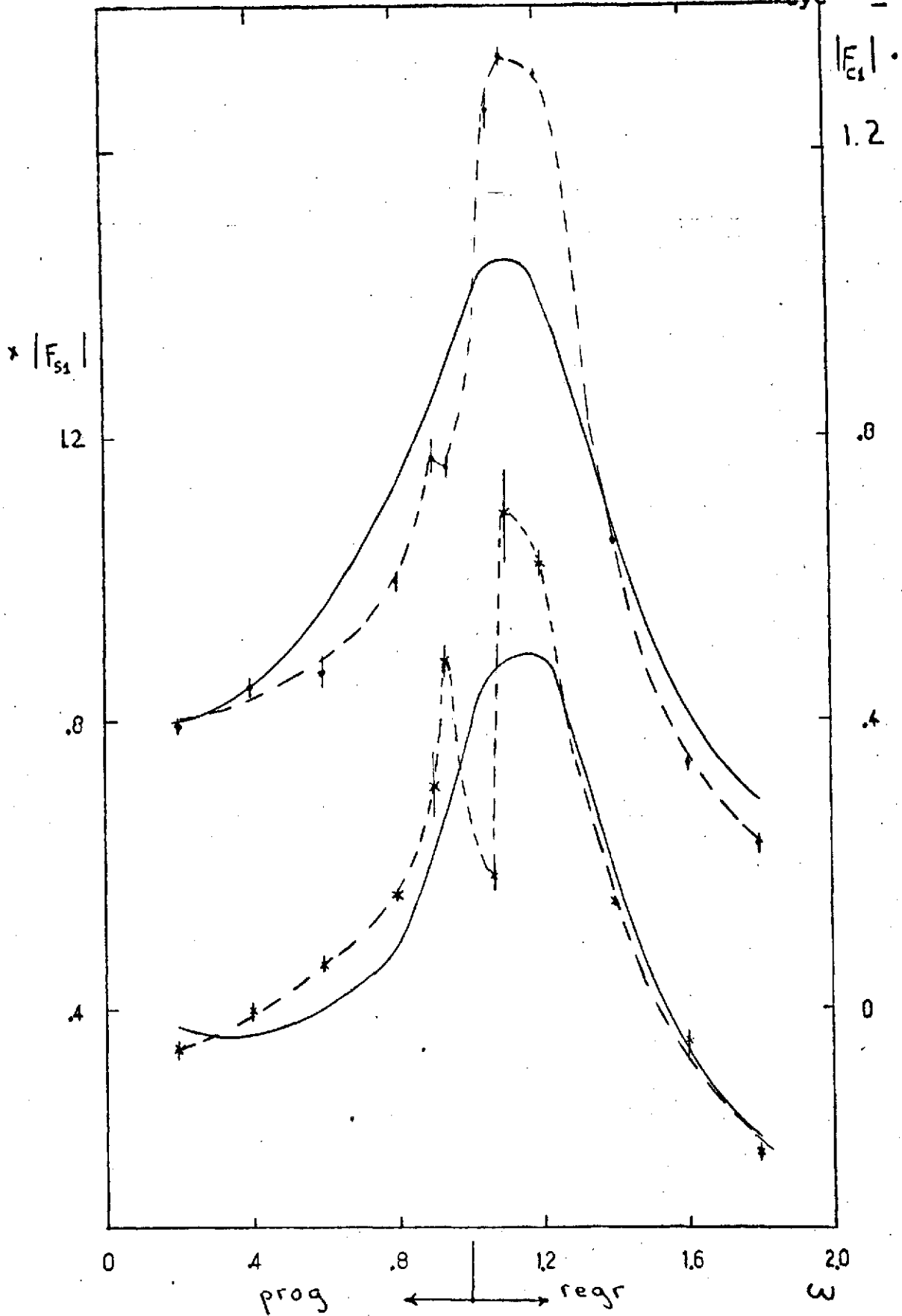


Fig. 13b

$$\mu = .4$$

$$P = 1.20$$

$$\theta_0 = 5^\circ$$

$$\theta_{cyc} = \pm 1.5^\circ$$

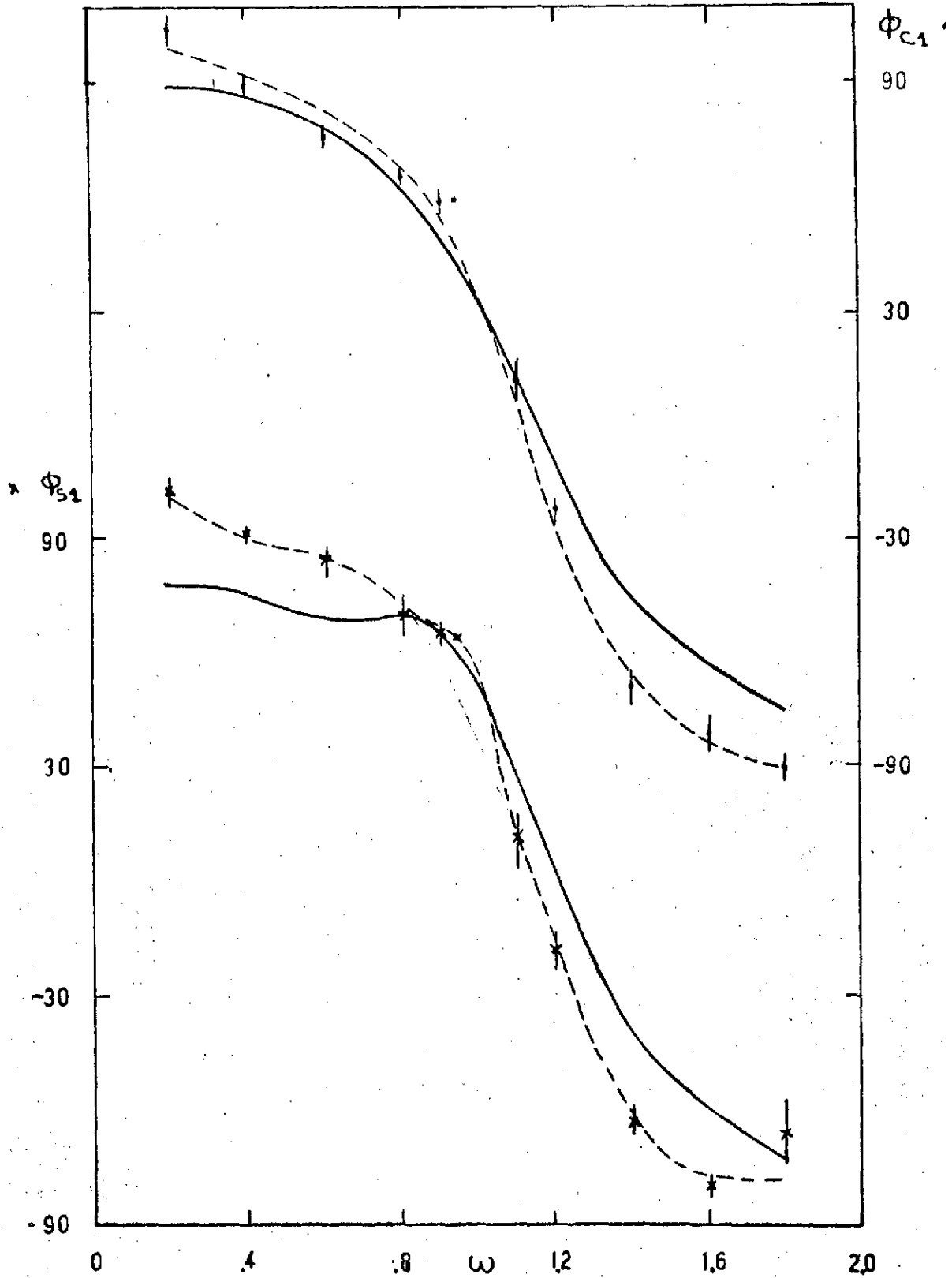


Fig. 13c

$\mu = .4$
 $P = 1.20$
 $\theta_0 = 5^\circ$
 $\theta_{cyc} = \pm 1.5^\circ$

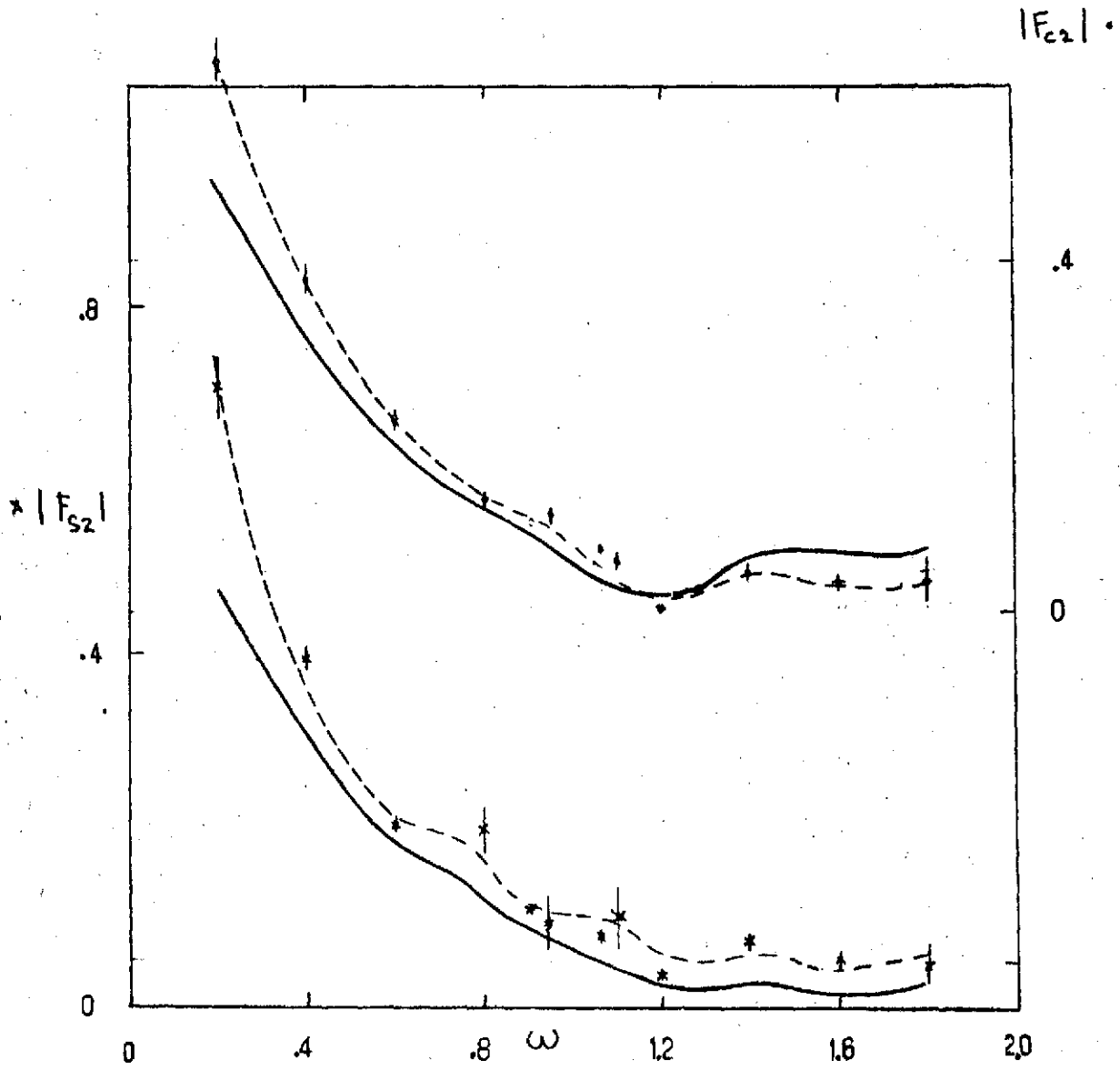


Fig. 13d

$\mu = .4$
 $P = 1.1$
 $\theta_o = 5^\circ$
 $\theta_c = \pm 1.5$

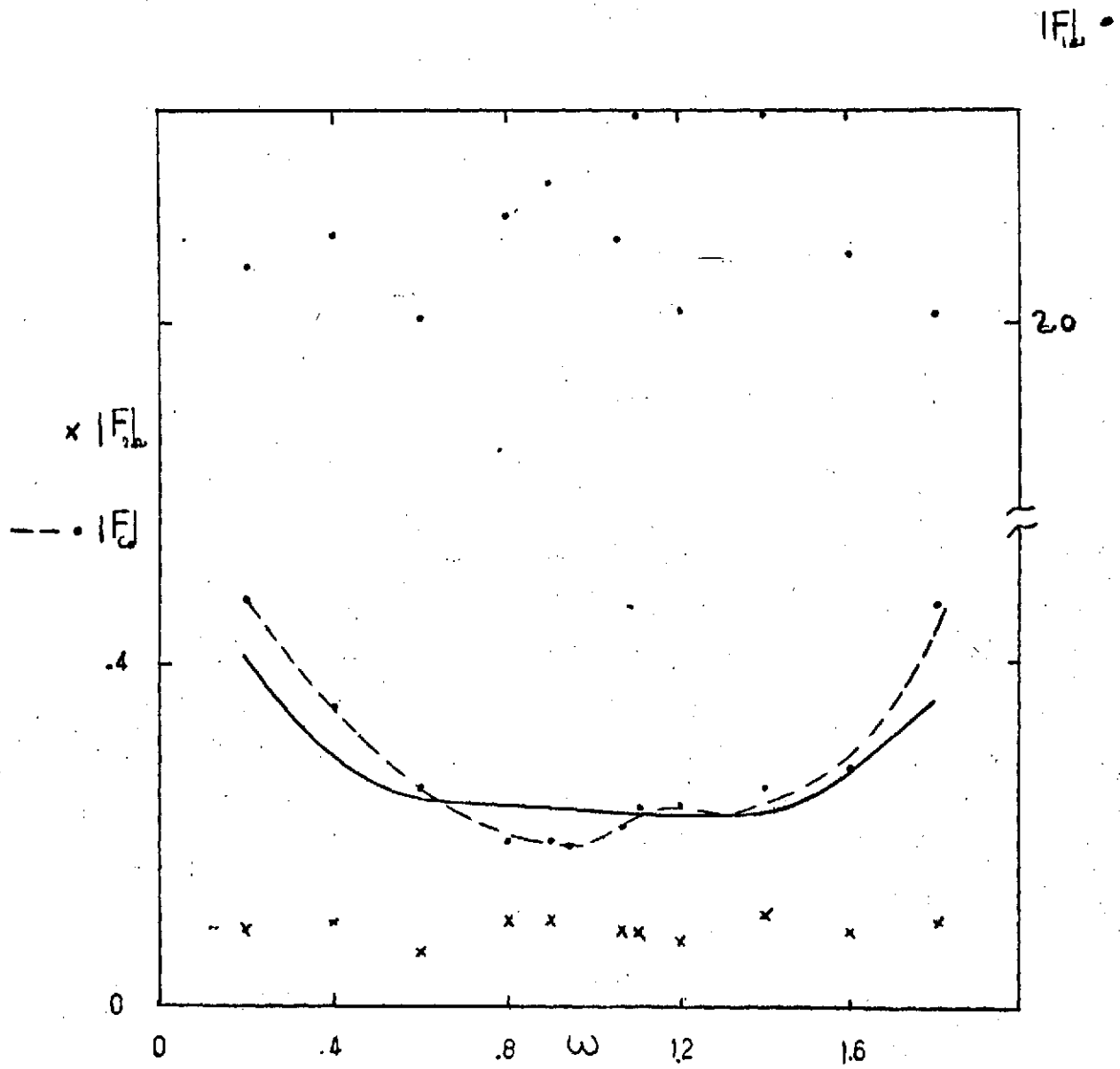
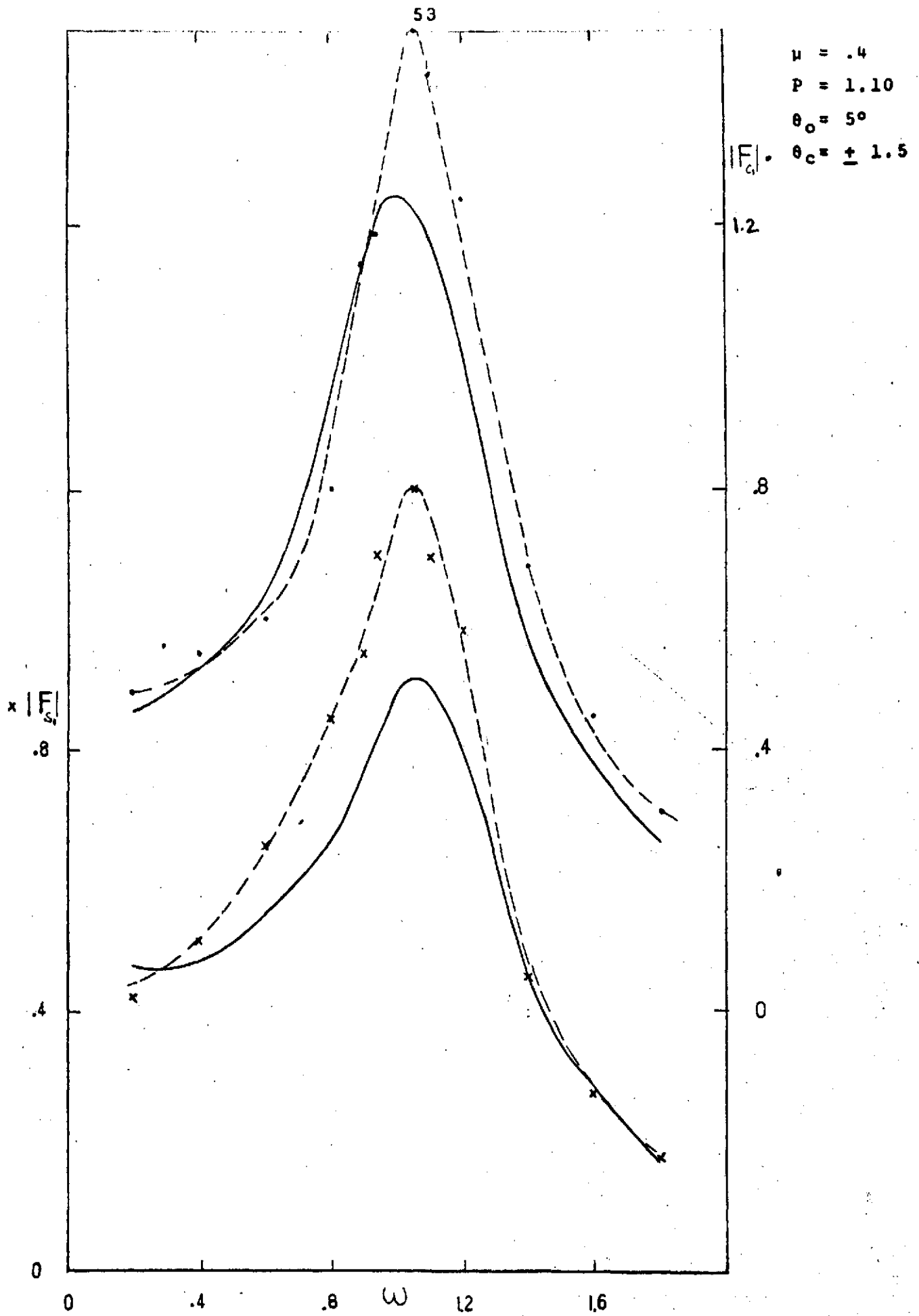


Fig. 14a



$\nu = .4$
 $P = 1.10$
 $\theta_o = 5^\circ$
 $\theta_c = \pm 1.5$

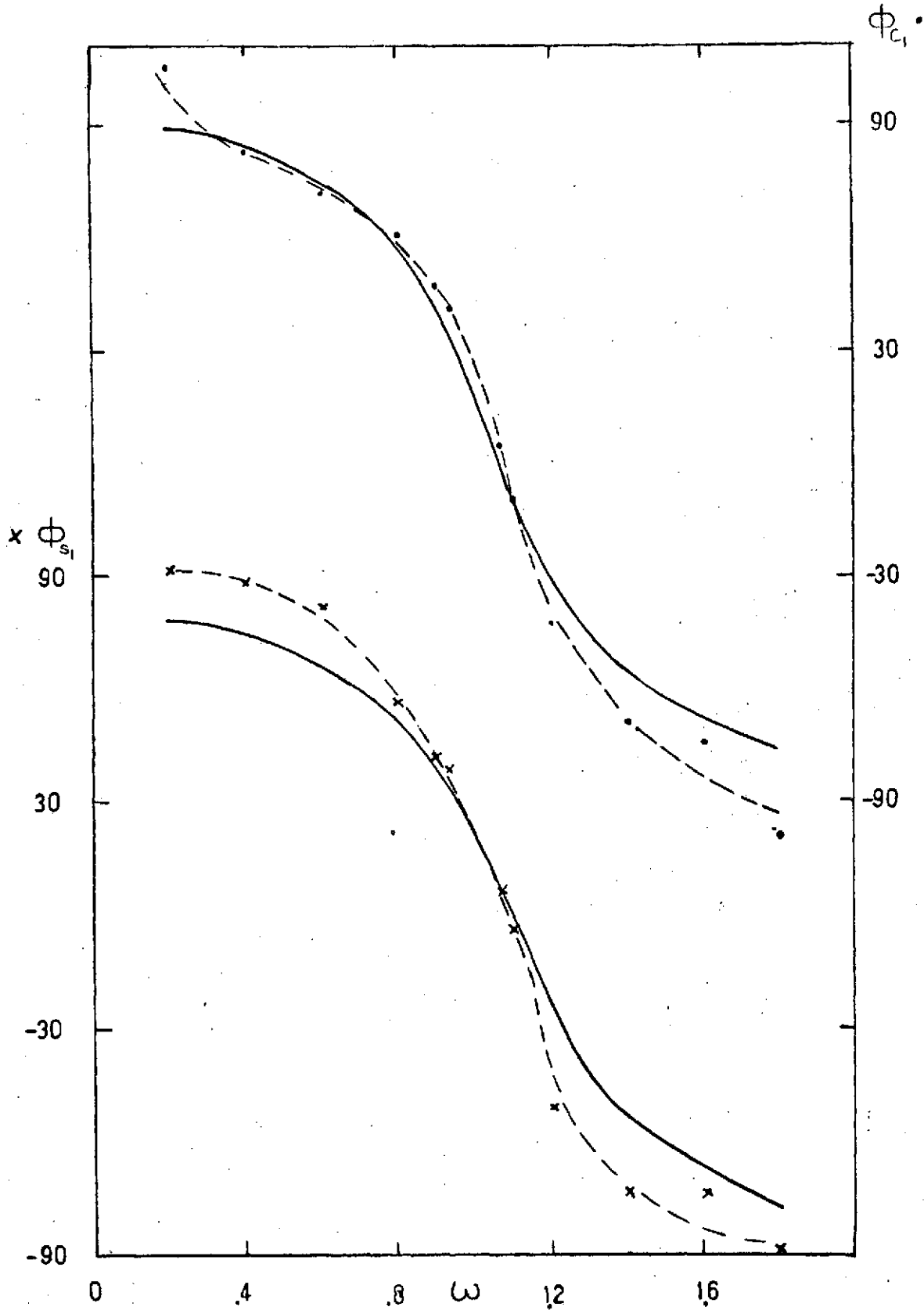


Fig. 14c

$\mu = .4$
 $P = 1.1$
 $\theta_0 = 5^\circ$
 $\theta_c = \pm 1.5$

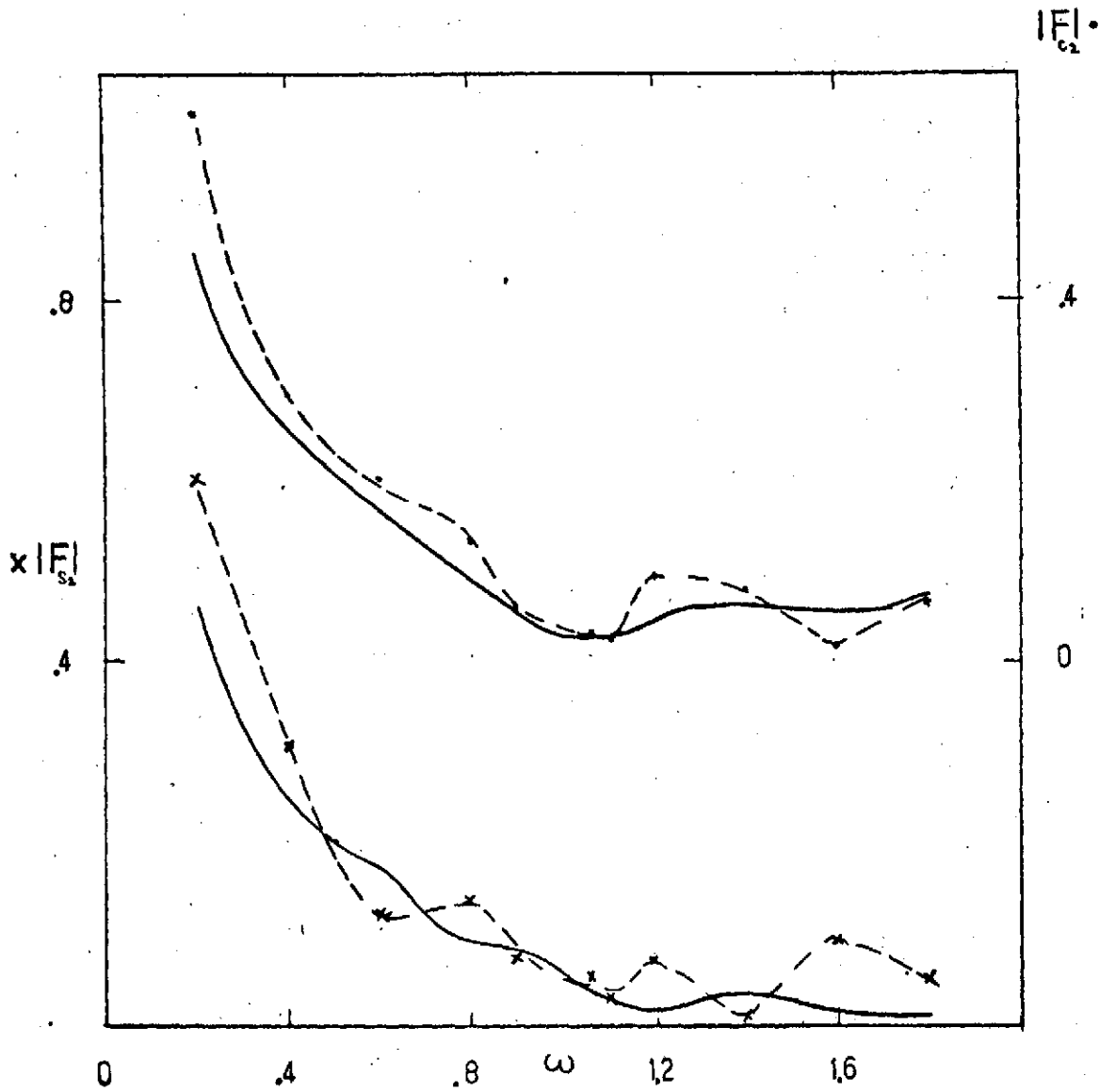


Fig. 14d

$\mu = .6$
 $P = 1.20$
 $\theta_0 = 2^\circ$
 $\theta_c = \pm 1.5^\circ$

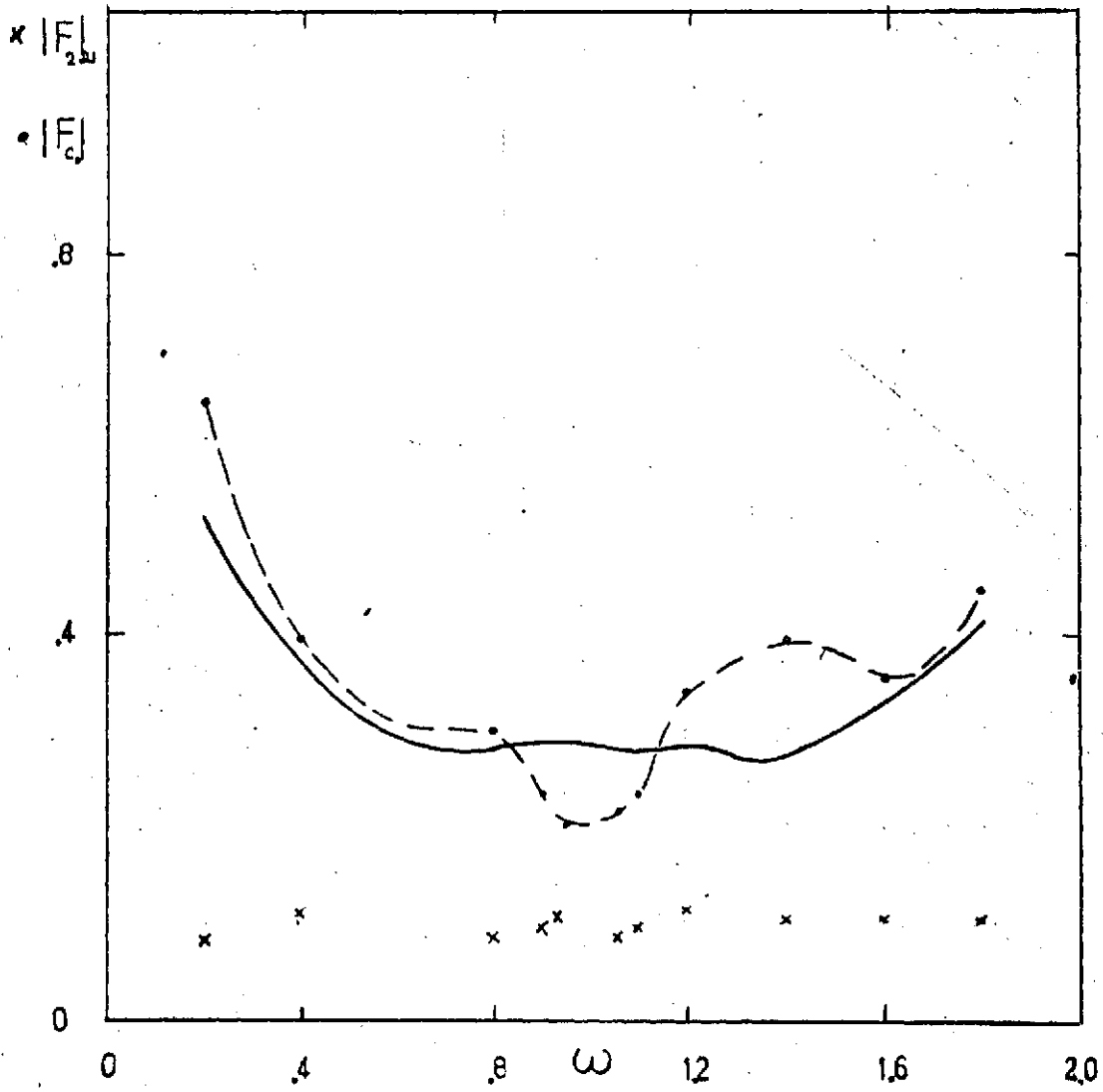


Fig. 15a

$\mu = .6$
 $P = 1.20$
 $\theta_0 = 2^\circ$
 $\theta_c = \pm 1.5^\circ$

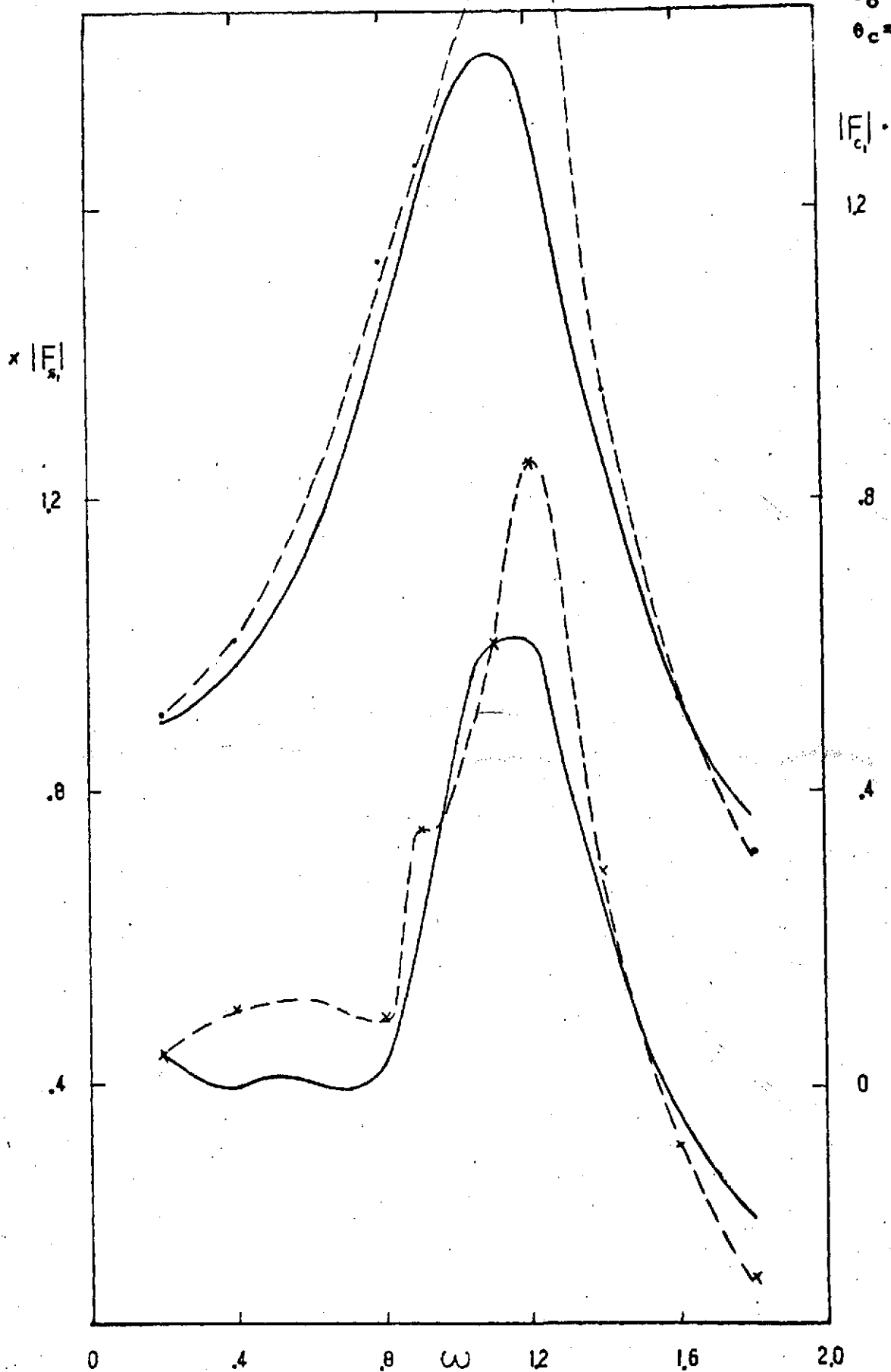


Fig. 15b

$\mu = .6$
 $P = 1.20$
 $\theta_o = 2^\circ$
 $\theta_c = \pm 1.5^\circ$

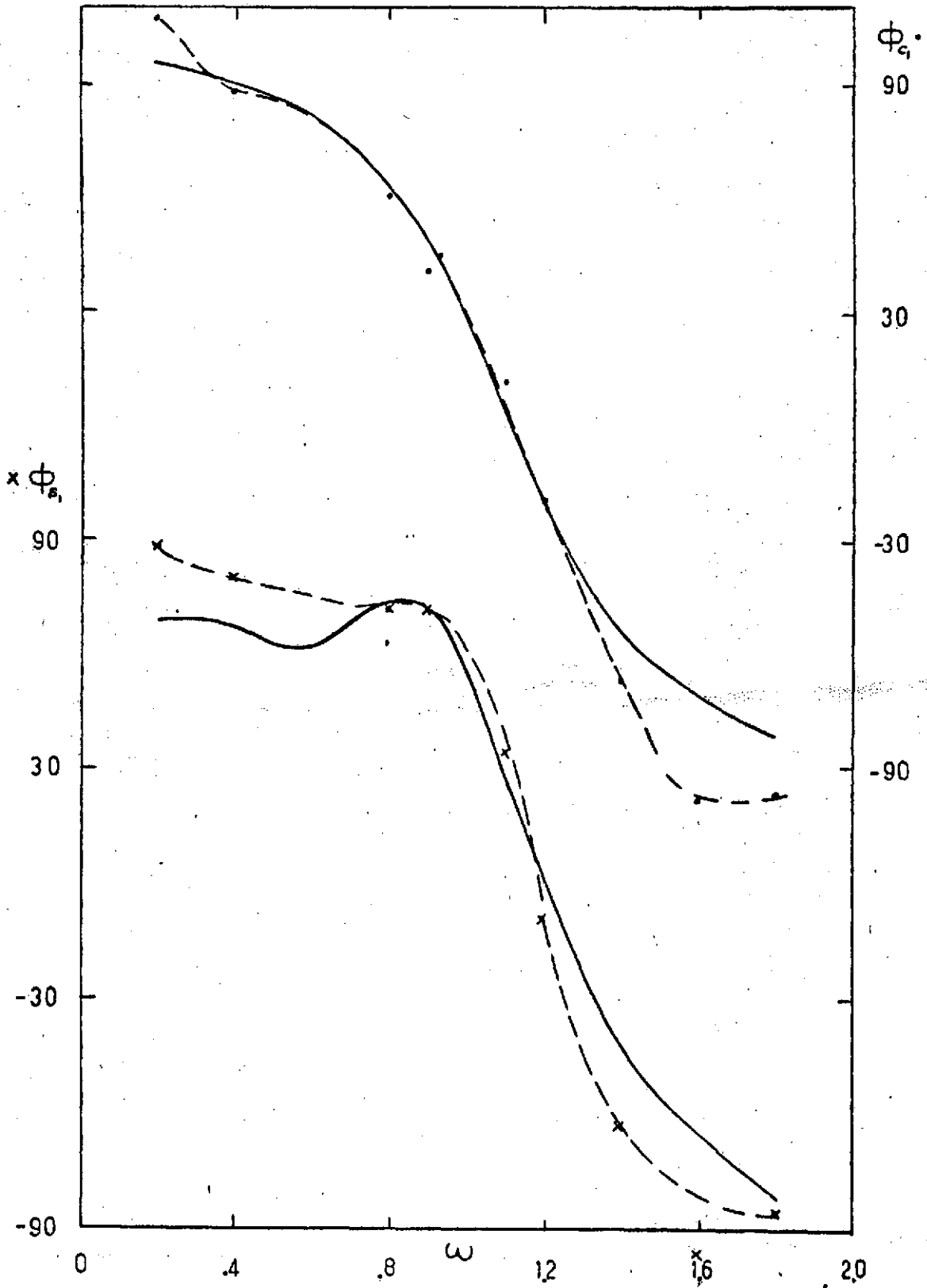


Fig. 15c

$\nu = .6$
 $P = 1.20$
 $\theta_0 = 2^\circ$
 $\theta_c = + 1.5^\circ$

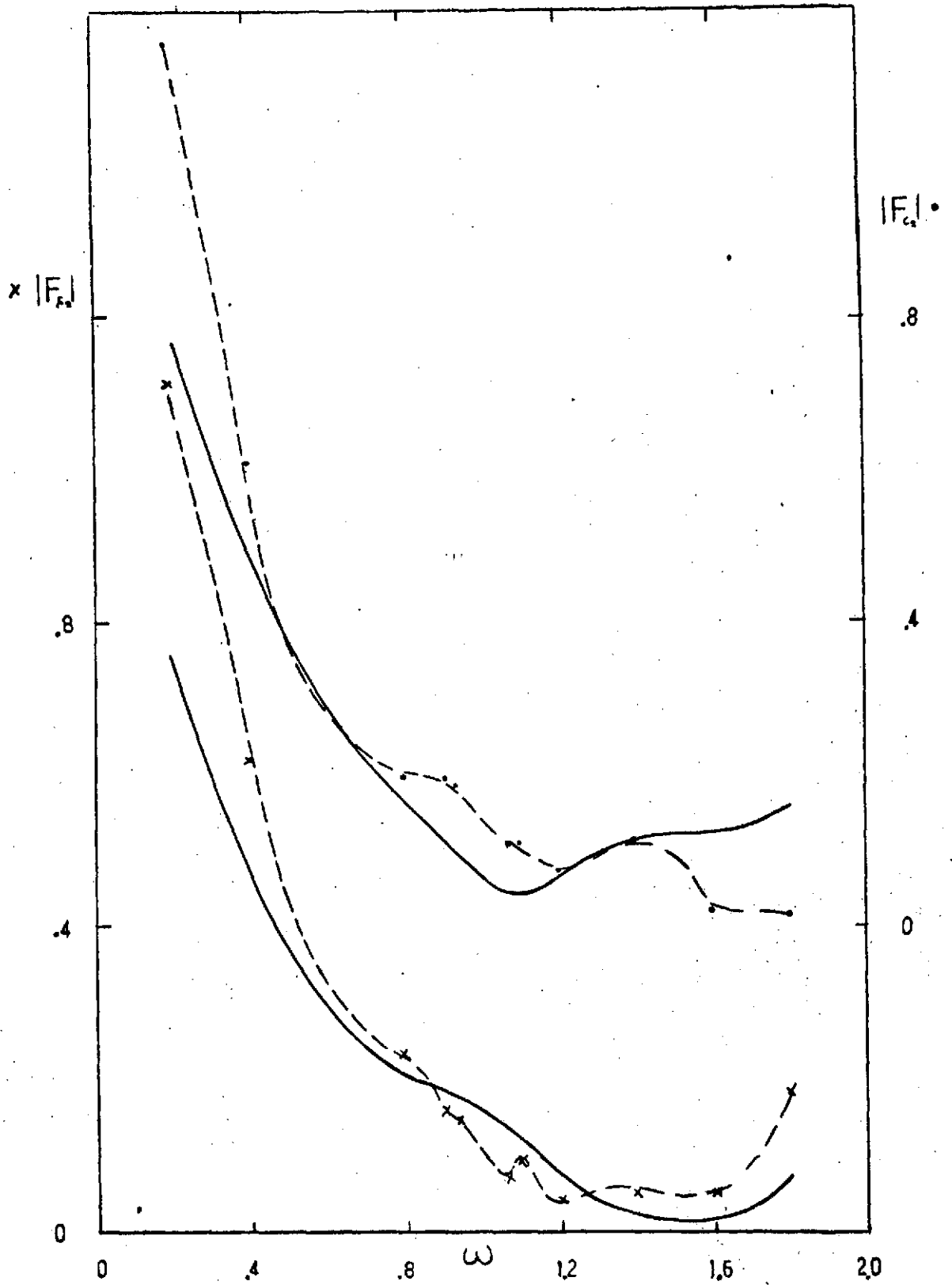


Fig. 15d

$\mu = .8$
 $P = 1.20$

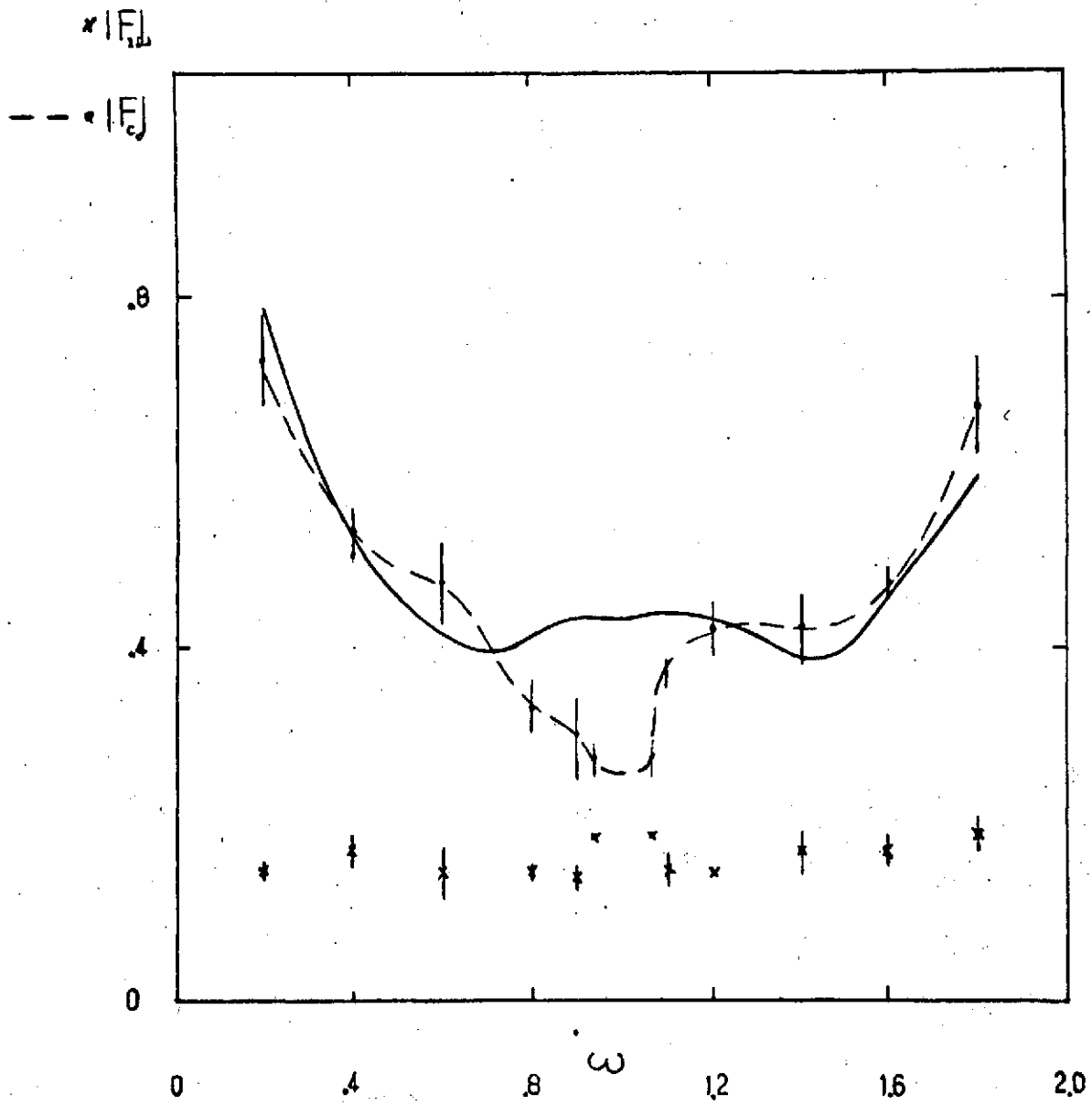


Fig. 16a

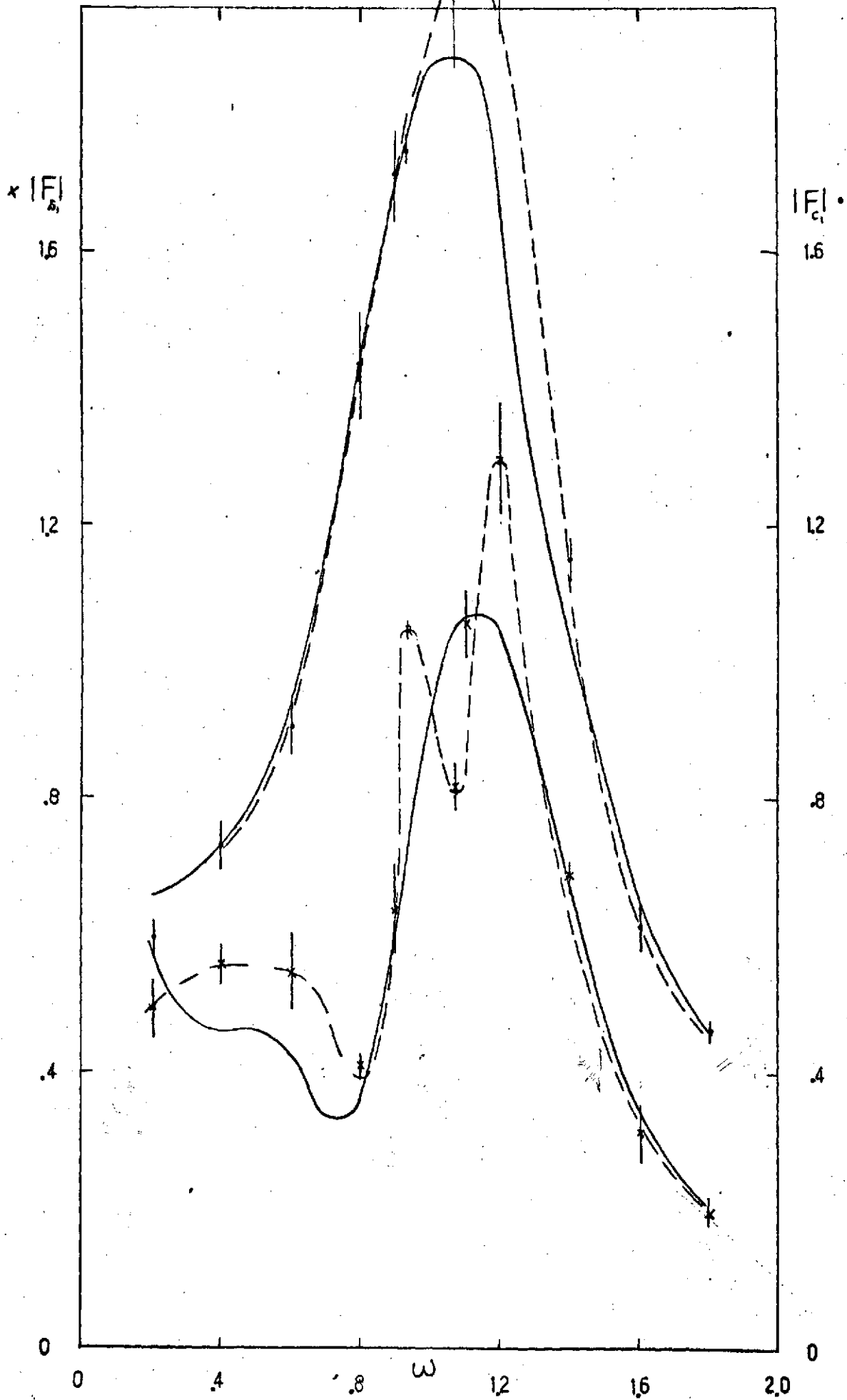


Fig. 16b

$\mu = .8$
 $P = 1.20$
 $\theta_o = 2^\circ$
 $\theta_c = \pm 1.5^\circ$

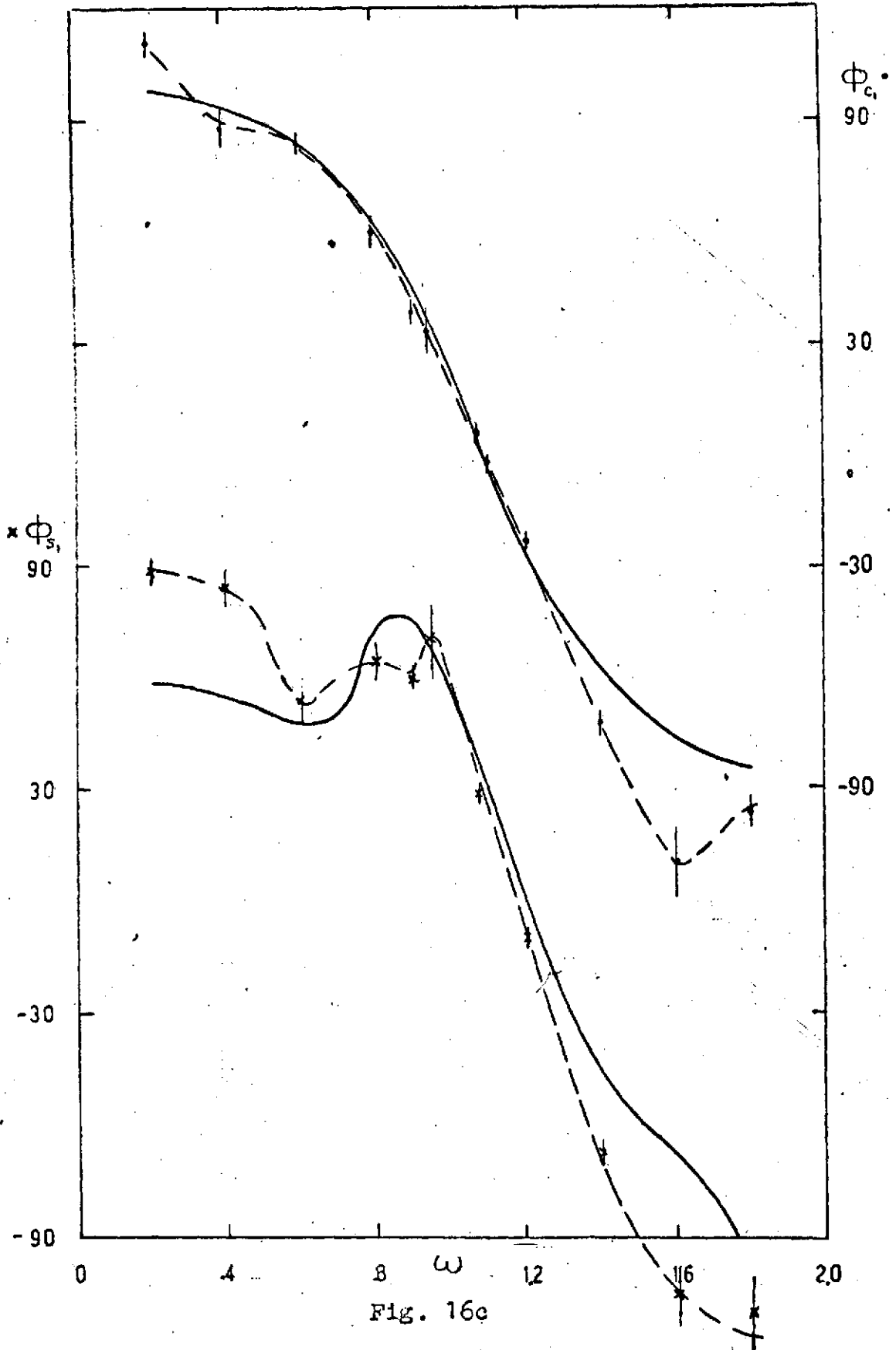


Fig. 16c

$\mu = .8$
 $P = 1.20$
 $\theta_0 = 2^\circ$
 $\theta_c = \pm 1.5$

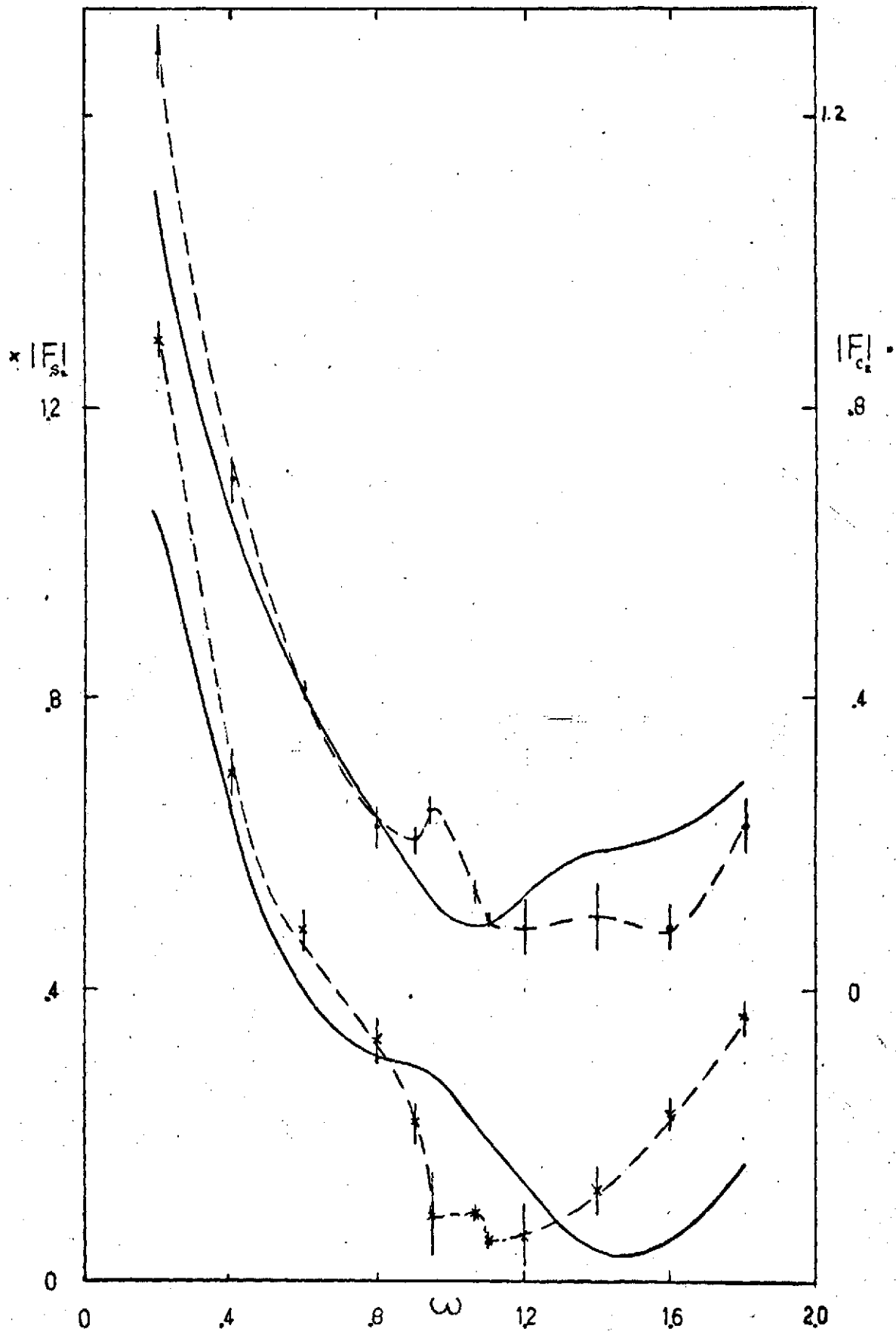


Fig. 16d

Figure 17 Side View-Pitch Stirring Rotor

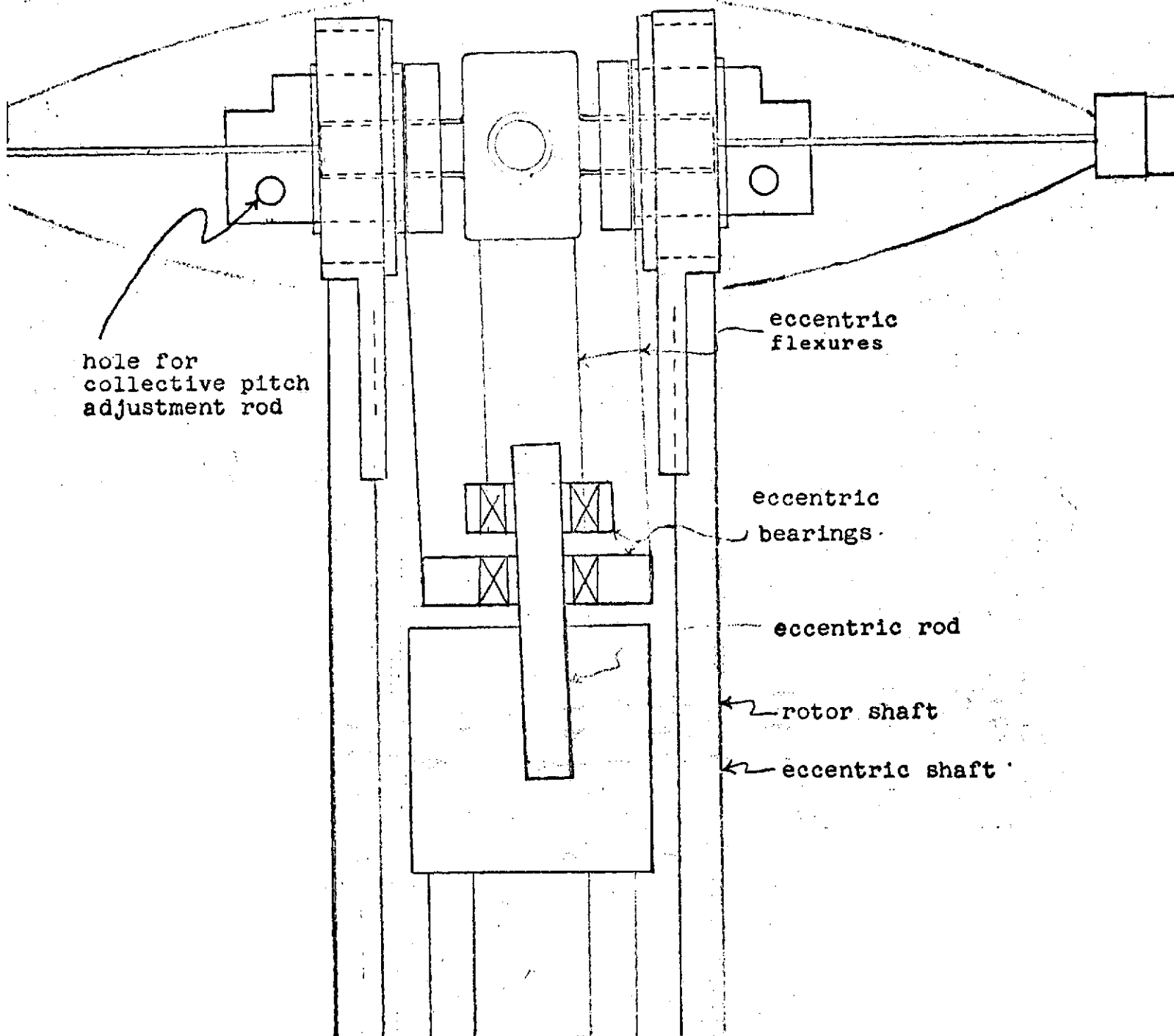
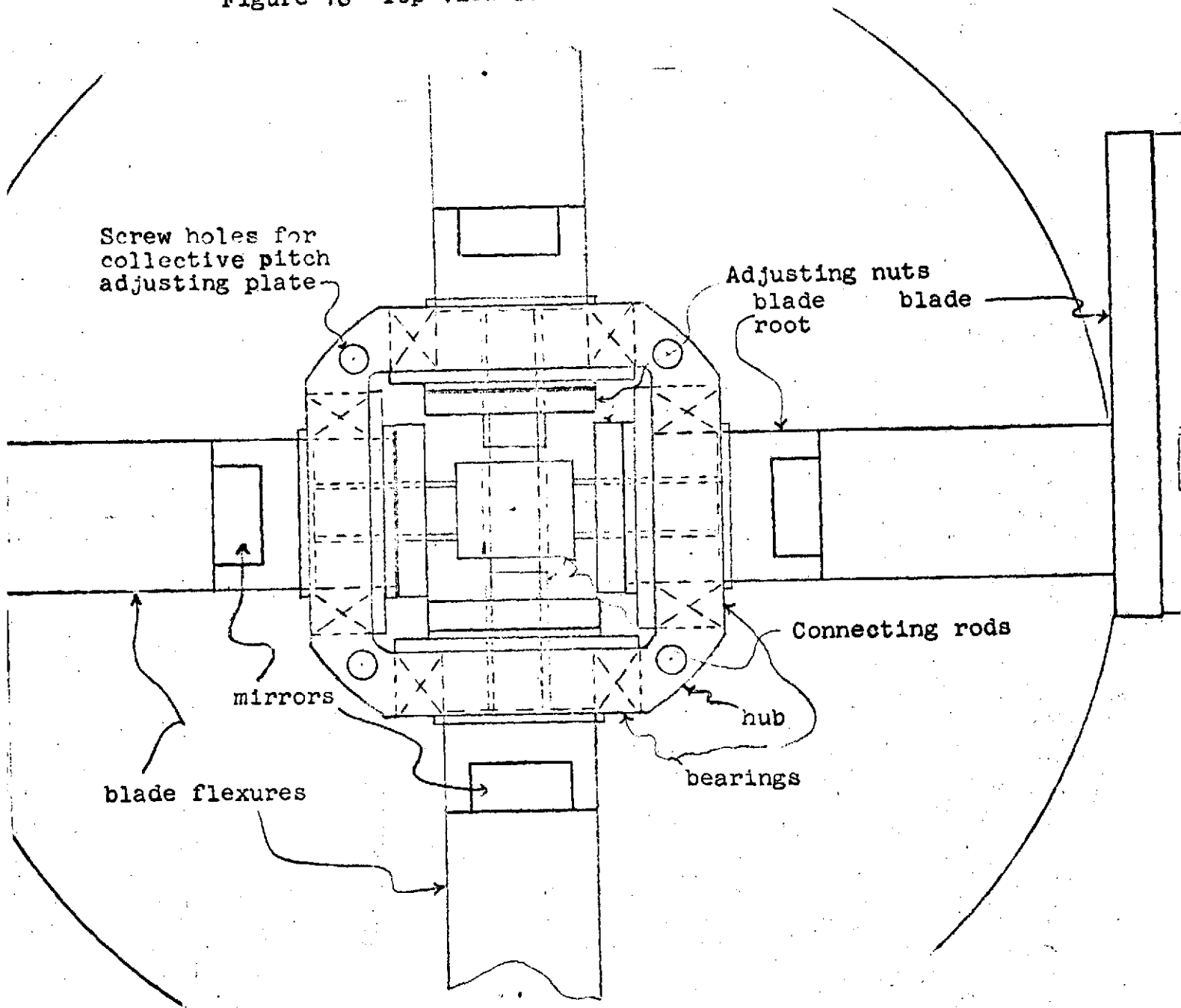


Figure 18 Top View-Pitch Stirring Rotor



Appendix AList of Purchased and Borrowed Equipment

In addition to the equipment listed in Reference 1 the following equipment was purchased and borrowed in FY 1973.

I. Purchased Equipment over \$1,000

1 - TSI Thermo Systems Incorporated Model 1050 Research Anemometer	\$1,285.00
2 - TSI Model 1052 Polynomial Linearizers at \$1,150 each	2,300.00
1 - TSI Model 1015C Correlator	1,075.00
Sum	<u>\$4,660.00</u>

This equipment is supplemented to equipment from the same company available at Washington University

II. Purchased Equipment under \$1,000 and over \$50

1 - TSI Model 1063 Sum + Diff. Circuit	\$295.00
1 - TSI Model 1058-12F Cabinet	195.00
1 - TSI Model 1156 Probe Holder	75.00
1 - TSI Model 1057 Signal Conditioner	645.00
1 - EMI Model 1540-P4 Oscillator Delay Unit	270.00
1 - EMI Model 1540-P2 Strobolume Lamp	265.00
1 - EMI Model 1536-A Photoelectric Pickoff	102.00
Sum	<u>\$1,557.00</u>

III. Borrowed Equipment - over \$1,000

1 - TSI Single Channel, non-linearized hot wire anemometry system (New value)	\$3,600.00
1 - Analog Computer (New value)	\$17,000.00